Advances in Applied Energy 14 (2024) 100168

Contents lists available at ScienceDirect

Advances in Applied Energy

journal homepage: www.elsevier.com/locate/adapen

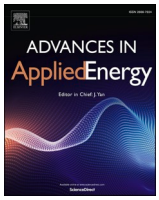

Current challenges in the utilization of hydrogen energy-a focused review on the issue of hydrogen-induced damage and embrittlement

Binhan Sun [a,*], Huan Zhao [b], Xizhen Dong [c], Chaoyi Teng [d], Aochen Zhang [a], Shuai Kong [a], Jingjing Zhou [a], Xian-Cheng Zhang [a], Shan-Tung Tu [a,*]

[a] Key Laboratory of Pressure Systems and Safety, Ministry of Education, School of Mechanical and Power Engineering, East China University of Science and Technology, Shanghai 200237, China
[b] State Key Laboratory for Mechanical Behavior of Materials, Xi'an Jiaotong University, Xi'an 710049, China
[c] Max-Planck-Institut für Eisenforschung GmbH, Max-Planck-Straße 1, Düsseldorf 40237, Germany
[d] AECC Beijing Institute of Aeronautical Materials, Beijing Key Laboratory of Aeronautical Materials Testing and Evaluation, Beijing 100095, China

ARTICLE INFO

Keywords:
Hydrogen embrittlement
Hydrogen energy
Hydrogen safety
Metallic materials
Hydrogen-induced damage

ABSTRACT

The development of reliable and longevous infrastructures and structural components is the key for the implementation of a hydrogen economy that is currently enjoying unprecedented political and research momentum due to the globally strong demand for clean energy. This is, however, strongly impeded by the risk and concerns of hydrogen embrittlement (or hydrogen-induced degradation in mechanical properties) that generally exists in almost all metallic materials. Structural components and materials operated in the hydrogen production-transport-storage-usage chain can be subjected to a very wide range of temperature, environmental and loading scenarios, which will essentially trigger different hydrogen embrittlement responses and even different embrittling mechanisms. It is thus important to have a systematic assessment and discussion of hydrogen embrittlement behavior of different materials at different testing conditions, which is the focus of the presented review. Here we cover the typical materials (mainly metallic materials) that have been used or planned to be used in the fields of hydrogen energy. We first briefly summarize the current understanding of fundamental hydrogen embrittlement mechanisms in metallic materials and the research progress in recent years. Then we analyze and discuss the hydrogen -induced damage phenomenon in typical materials used in the field of high-pressure hydrogen transport and storage. In addition to room-temperature hydrogen embrittlement behavior, the hydrogen embrittlement phenomenon of some alloys at elevated and cryogenic temperatures is also reviewed, with the aim to provide some guidelines of material selection and design in developing fields such as hydrogen gas turbines and long-flight-duration hydrogen powered aircraft. Finally, the current challenges in the study of hydrogen embrittlement are identified and discussed to guide future research efforts.

Introduction

There is no doubt that hydrogen (H) is becoming one of the most promising sustainable energy carriers which can release at least partially the current strong reliance on fossil fuel-based energy and the resulting environmental burden. H can be produced from a variety of sources (either hydrocarbon or non-hydrocarbon) and can be utilized in many industrial and transportation fields. It can be stored in a large quantity and is relatively easy to transport over long distances. Further, H is environmentally benign, recyclable and reactive [1]. These advantages of H have long been recognized by researchers which has led to the idea of H economy. This concept, initially proposed in 1968 [2], describes a vision of utilizing H to store and transport energy produced from renewables (e.g. nuclear, wind or solar sources). It is currently enjoying unprecedented political and research momentum, with the number of policies and projects around the world expanding rapidly, which is driven by the increasing concerns of greenhouse gas emission. Obviously, the realization of H economy will have enormous impact and technical appeal for the decarbonization that is urgently required based on global commitments of the 2016 Paris Agreement. According to the report "Net Zero by 2050: a Roadmap for the Global Energy Sector [3]", the use of H and H-based fuels is expected to grow sixfold from today's

* Corresponding authors.
E-mail addresses: binhan.sun@ecust.edu.cn (B. Sun), sttu@ecust.edu.cn (S.-T. Tu).

https://doi.org/10.1016/j.adapen.2024.100168
Received 30 December 2023; Received in revised form 16 February 2024; Accepted 19 February 2024
Available online 22 February 2024

levels to meet 13 % of worldwide total final energy consumption in 2050. This is a challenging mission that requires to overcome quite a few long-standing obstacles, with one being the safety and longevity of key infrastructures and structural components needed for the implementation of a H economy.

While H provides a variety of benefits as an efficient and clean energy carrier, it causes one of the most dangerous and yet most elusive embrittlement problems for metallic materials [4]. Due to the small and ubiquitous nature of H atoms, they can easily enter into a metal through surface physical adsorption followed by chemisorption and/or simply electrochemical reaction, causing an abrupt loss of a material's load-bearing capacity even when the overall H concentration is as low as a few wt ppms [4–10]. This phenomenon, known as H embrittlement (HE), results in serious degradation of metals' mechanical properties, mainly in terms of ductility, toughness and fatigue resistance [11]. It should be noted that the term of HE represents an overall deterioration of materials' mechanical properties and does not necessarily mean that the fracture mode is becoming brittle [4]. Nevertheless, the H-induced catastrophic failure of materials essentially leads to unexpected H_2 leaks that can cause combustion and explosion due to the low-ignition energy and wide flammability range of H_2 [12].

Since the first observation of HE in 1875 [13], the extensive study in the past 100 years has revealed the occurrence of such phenomenon in most mass-produced metallic materials, including those used in H storage and transport infrastructures and in H power plant (e.g. Cr-Mo steels [14], stainless steels [14], Al alloys [15], superalloys [16], etc.). The issue of HE in these materials renders difficulties and strong concerns for the design of H-related structural components, especially pertaining to the selection of proper materials and their service life prediction in H abundant atmosphere. Currently, the fundamental mechanisms for HE are still not clear and vary with different materials. This inhibits the development of reliable life prediction models from a physics-based "bottom-up" approach. However, it would still be valuable to conduct a phenomenological yet systematic analysis on the HE behavior of typical materials that can be potentially used in the chain of H economy, which is the main focus of the presented review. Here, we mainly address the H-induced damage phenomena and the resulting HE susceptibility in materials with a target application in H storage, transport, power generation and engines. The influence of various microstructural, testing and environmental factors on HE of these materials is also systematically analyzed. In addition, the fundamental HE micromechanisms operated in these materials are covered. Given that the latter subject has been thoroughly discussed in recent reviews [4, 17–19], here we mainly focus on the associated progress in the last a few years. The current investigation challenges in the field of HE and their impact on the utilization of H energy will also be summarized in the last section of this review.

Recent progress in the study of H embrittlement mechanisms

It is generally accepted that the occurrence of HE in metallic materials involves three processes: (a) the ingress of H atoms from the H-containing atmosphere, followed by its diffusion (even at room temperature) to stress-concentrated fields and microstructural traps; (b) the interaction between H atoms and a variety of multi-dimensional microstructural defects including vacancies, solute atoms, dislocations, interfaces and micro-voids/cracks [20]; (c) the promoted damage nucleation and evolution due to the H-defect interactions. The specific mechanisms for the latter two HE processes are subjected to the most controversies, which is reflected by the existence of a variety of different embrittlement models, e.g. H-enhanced decohesion (HEDE) [21], H-enhanced localized plasticity (HELP) [22], H-enhanced strain-induced vacancies (HESIV) [23] and adsorption-induced dislocation emission (AIDE) [24] (schematically summarized in Fig. 1). These HE mechanisms have already been comprehensively discussed in recent reviews [4,18,24–26], thus here we only provide a brief description with more focuses placed on the recent progress and existing issues. The HEDE model describes that the presence of H reduces the cohesive strength of lattice planes or interface boundaries [27,28], which promotes a pure brittle fracture behavior by the facilitated crack nucleation and propagation along certain crystal planes and interfaces [7,27–29]. The HELP model is inherently a plasticity-associated "embrittlement" mechanism, which proposes that the H-enhanced localized deformation can make the material readily achieve the plasticity limit thus promoting the formation and evolution of damage at local regions (e.g. near crack tips). The original framework of the HELP mechanism mainly discusses the effects of internal H on dislocation mobility which is associated with the influence of H atoms on dislocation-obstacle

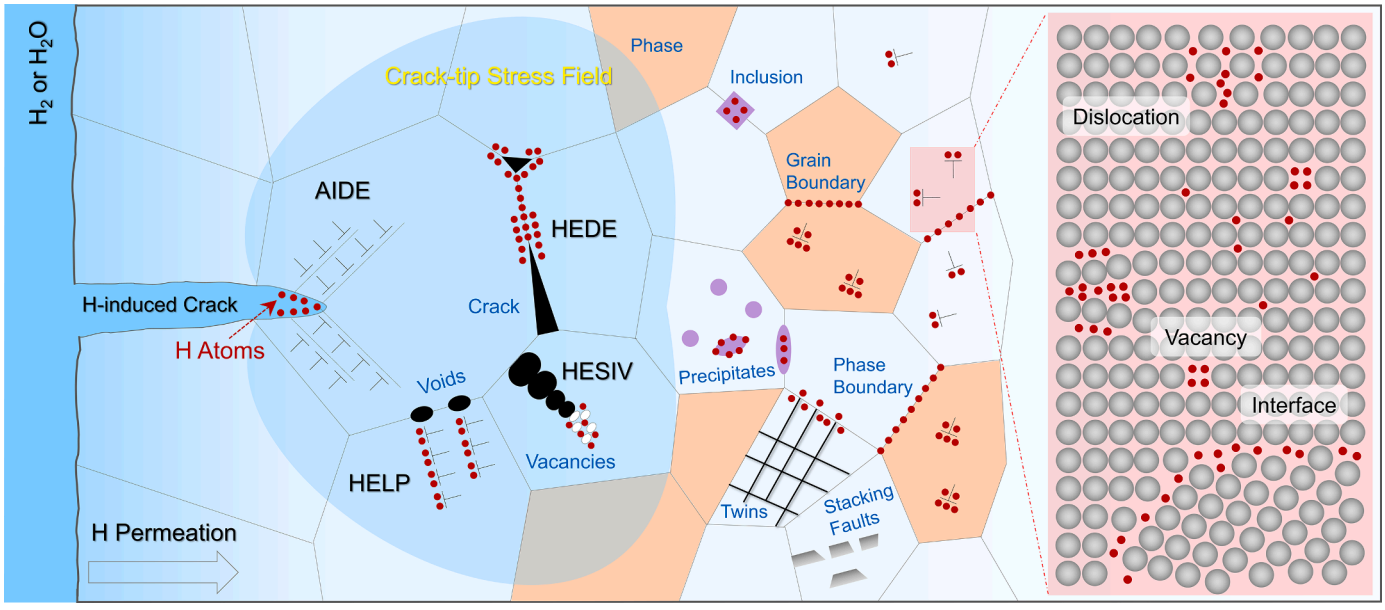

Fig. 1. Schematic diagram showing the interaction between H atoms and some of the microstructural defects as well as commonly reported H embrittlement models (HEDE: H-enhanced decohesion, HELP: H-enhanced localized plasticity, AIDE: adsorption-induced dislocation emission, HESIV: H-enhanced strain-induced vacancies).

interactions [30–32], the Peierls stress [33] or kink nucleation energy [34]. On the other hand, the AIDE model highlights the influence of surface-absorbed H on promoting dislocation emission at the crack tips (due to the adsorption-induced weakening of interatomic bonds), which subsequently facilitates crack advances [24,25]. Unlike the HELP and AIDE models that are developed based on H-dislocation interactions, the HESIV mechanism addresses the influence of H atoms on stabilizing strain-induced vacancies which can further promote the formation of vacancy clusters and subsequent small nano-sized voids [35–37].

It is worthwhile to be noted that despite different views on HE micromechanisms as described above, they do not repel each other and the main controversies lie in the generality and prevalence (or contribution) of certain mechanisms on H-induced premature failure. In fact, there is currently an increasing number of researchers accepting a hybide HE mechanism involving a combination of various micromechanical models and their interplay [6,24,29,38]. For instance, the enhanced dislocation activity due to HELP might promote the formation of strain-induced vacancies and activate the HESIV mechanism [6,24]. The higher density of pile-up dislocations due to the HELP effect might facilitate H transport to the obstacles (e.g. interfaces) thus promoting the occurrence of the HEDE effect [38,39]. The HEDE effect at the precipitate-matrix interfaces would promote void nucleation ahead of the propagating crack tip no matter what mechanisms (HELP or AIDE) drive the crack propagation [40].

The main reason accounting for the controversies among the above-mentioned HE models is the lack of convincing experimental evidences. Although some HE mechanisms (e.g. HEDE and HELP) have been extensively studied for decades, the corresponding evidences still largely remain indirect and/or non-statistical. The main challenges lie in the experimental difficulty of visualizing H atoms, their migration/trapping and interactions with microstructural defects. The dynamic and multi-dimensional nature of HE also requires experiments/simulation to cross various length and time scales, which is still a strong challenge today. Therefore, the development of experimental and modelling tools is the key to unravel the HE mechanisms. In this context, notable progress has been achieved in recent years, as elaborated upon in the subsequent sections.

The characterization of H atoms is probably the most challenging

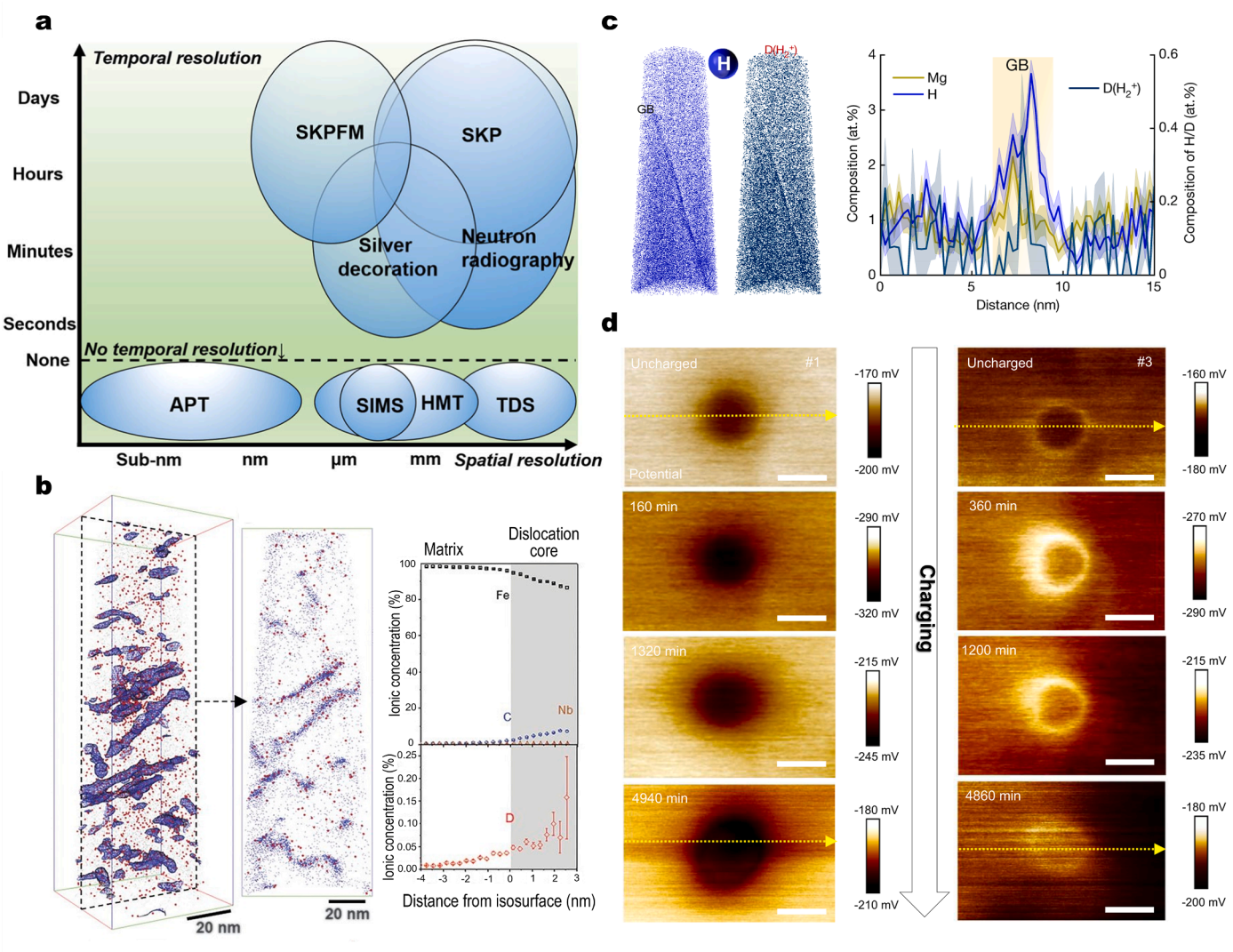

Fig. 2. (a) Temporal and spatial resolution regimes of commonly used H probing techniques [47]; (b) APT results of a d-charged microalloyed martensitic steel, showing D enrichment at dislocations [48]. The 2 at.% C isoconcentration surfaces (in blue) are used to mark dislocation lines. The collective proxigram analysis of the observed dislocations in the dataset is shown on the right side; (c) APT results of a d-charged peak-aged Al-Zn-Mg-Cu sample containing a grain boundary, with one-dimensional solute profile across the grain boundary plotted on the right side [15]; (d) SKPFM potential maps of a low-alloyed martensitic steel at uncharged state and sequential H-charged states (for different times from 160~4900 min), showing different H trapping behavior between two precipitates with incoherent interfaces with the matrix [55].

task, yet often the very first step, to understand H-induced damage. The small, highly diffusible and ubiquitous nature of H poses a strong challenge for modern characterization techniques to achieve both high resolution and high fidelity. Commonly used microstructure-sensitive H probing techniques include thermal desorption spectrometry (TDS) [41], H microprint technique (HMT) [42], secondary ion mass spectroscopy (SIMS) [43], scanning Kelvin probe (SKP) [44], scanning Kelvin probe force microscopy (SKPFM) [44], neutron radiography/tomography [45] and atom probe tomography (APT) [46]. The respective temporal and spatial resolution of these techniques are summarized in Fig. 2(a), with more details overviewed in Ref. [47]. In particular, APT and SKPFM have the highest spatial resolution that allows to reveal the H trapping behavior in fine microstructural features (e.g. nano-sized precipitates, dislocations and interfaces). Some interesting finding has recently been reported in this aspect. For example, Chen et al. [48] have studied the H trapping behavior of a Nb-bearing low-C martensitic steel using APT. The needle-shaped APT samples were charged with deuterium (D) to avoid the interference of environmental H, after which they were transferred into the measurement chamber via a cryogenic chain with the aim to minimize H/D desorption. Results have revealed the enrichment of D/H at C-rich dislocations (as shown in Fig. 2(b)) as well as at grain boundaries and carbide-matrix interfaces. Zhao et al. [15] focused on a high-strength 7xxx Al alloy, using a slightly different APT experimental route. Instead of applying cryogenic sample transfer, they have prepared the APT tips from a D pre-charged bulk specimen by plasma focused-ion beam (PFIB) conducted at cryogenic temperatures. This can also suppress H egress. Through the subsequent data analysis, they observed strong partitioning of H into the second-phase particles (i.e. the S phase and Al_3Zr dispersoid) and co-segregation of Mg and H atoms at grain boundaries (Fig. 2(c)). The latter phenomenon was shown to be the main factor for the observed H-induced grain boundary decohesion. In addition to the above two examples, APT studies have also been carried out on other metallic materials including Ti alloys [49,50], Zr alloys [51,52] and various types of high-strength steels [46,53,54]. These investigations provide detailed information of hydrides formation or direct evidence supporting the capability of certain microstructural features (precipitates, interfaces and dislocations) in H trapping. However, it should be noted that APT experimental procedures for H mapping are often very complicated, requiring a careful and delicate sample preparation, D/H charging, transfer and measurement [46]. Parameters for each experimental step are also highly dependent on the studied material. Inappropriate operation in any of these steps or unsuitable experimental parameters will result in failure of the whole experiments or disputed results. Other issues that might decelerate the development of APT in H probing is the strong challenges of accurate quantification of solute H atoms and the lack of temporal resolution.

SKPFM is another technique that has recently been used for mapping H [44,56]. Detailed description of such technique has been given elsewhere [44]. Compared with APT, SKPFM has a worse spatial resolution and only provides a two-dimensional information (Fig. 2(a)), but it offers dynamic information of H permeation and desorption and requires simpler sample preparation procedures. During the measurement, the accumulation of H at specific sites (phases or interfaces) allows a qualitative image of the H distribution represented by different contrast in the surface potential. One such example is shown in Fig. 2(d), which demonstrates the potential maps of two regions in a low-alloyed martensitic steel subjected to electrochemical H charging from the back side for different times (0~4900 min). A darker contrast (i.e. lower potential) implies a higher local H concentration. In this particular work [55], it was observed that incoherent Ti_2CS precipitates can show very different H trapping potency, namely, the precipitate/matrix interface can either trap H (left images in Fig. 2(d)) or reject H (right images in Fig. 2(d)). Subsequent focused-ion-beam (FIB)-transmission electron microscopy (TEM) and density function theory (DFT) studies suggested that such difference in interface H trapping was associated with vacancies at the precipitate surface and elastic strain of the matrix nearby the interface. Although the non-destructive SKPFM method allows the correlation between H enrichment/depletion and other microstructural information (local chemistry and structure), it is essentially a surface sensitive technique from which the data are influenced by the H migration through the bulk of the alloy and H desorption at the surface. Any local interruption of H migration routes between the charging side and the measurement side will lead to incorrect interpretation.

A full picture of the interactions between H and microstructural defects (e.g. vacancies, dislocations and interfaces) is another essential element that is required to understand HE. In this aspect, most research efforts have been devoted to the H-dislocation interaction. Early in ~1980s, researchers have conducted a series of *in-situ* transmission electron microscopy (TEM) experiments on a variety of materials (e.g. steels, Ni alloys, Al alloys, etc.) to directly observe the effects of H on dislocation gliding [57–59]. Results revealed an increasing dislocation mobility (regardless of the dislocation types), a reduced separation distance between pile-up dislocations and an enhanced tendency for dislocation planar slip, when tens of torrs of gaseous H_2 were introduced into the environmental cell [57–59]. These results later serve as the key experimental evidence supporting the HELP mechanism. However, debates continuously arise, especially pertaining to whether the previous *in-situ* TEM observations are affected by some sorts of artifacts (e.g. the bending stresses in the TEM foil introduced from the gas pressure or from the high H fugacity produced by the electron beam dissociating and ionizing the H) [25,60]. Indeed, some atomistic calculations have shown a rather decreasing effect of H on dislocation mobility (i.e. a strengthening effect) [61–63]. In view of these controversies, some advanced *in-situ* experiments have recently been designed to revisit the H-dislocation interactions [61,62,64], which is worthwhile to discuss.

The recently developed *in-situ* nanoindentation and environmental transmission electron microscopy (ETEM) are the two commonly discussed techniques for quantitatively revealing the H-dislocation interactions with high resolution. The *in-situ* nanoindentation method, first developed by Barnoush et al. [65,66], assists in probing the H effect on mechanical properties and simultaneously in detecting the H-affected dislocation behavior at the nanoscale. This technique has been used to investigate the HE mechanisms in many materials (e.g. pure Al [65], pure Cu [66], pure Ni [65,66], steels [67,68] and high entropy alloys [69,70]). Sample charging in the experimental setup can be conducted at either “back-side” (opposite to nanoindented surface) or “front-side” (at nanoindented surface), as shown in Fig. 3(a) [67]. It is worthwhile to mention that while the back-side charging method can prevent any possible contamination/degradation on the measurement surface, it might not be suitable for metallic materials with a slow H diffusivity (like austenitic steels) due to prolonged time required for H migrating through the whole thickness. Nevertheless, from the generated load-displacement curve, the influence of H on dislocation nucleation behavior (indicated by the occurrence of the pop-in phenomenon) and local mechanical properties (hardness and elastic modulus) can be evaluated. Regardless of the charging approach, a H-induced reduction in pop-in load (Fig. 3(b)) has generally been observed in a variety of materials (e.g. TWIP steel [68], CoCrFeMnNi high-entropy alloy [69] and Fe-Cr alloy [67]), although the extent of such reduction is dependent on composition, microstructure and grain orientation. Such phenomenon can be linked to the earlier onset of plasticity caused by H-promoted homogeneous dislocation nucleation [66,68], which was often explained in the concept of Defactant model [66,68]. It is proposed that H, act as a defactant, can reduce the formation energy of defects (e.g. dislocations) in a manner analogous to the case that surfactants reduce the surface energy of liquids [71–73]. In addition to the pop-in phenomenon, H also influences the nano-hardness value, with an increasing effect often reported (Fig. 3(c)) [67,68]. One argument attributed this to the H-associated Cottrell-like atmosphere formed around dislocations that can retard dislocation motion [61,70]. The

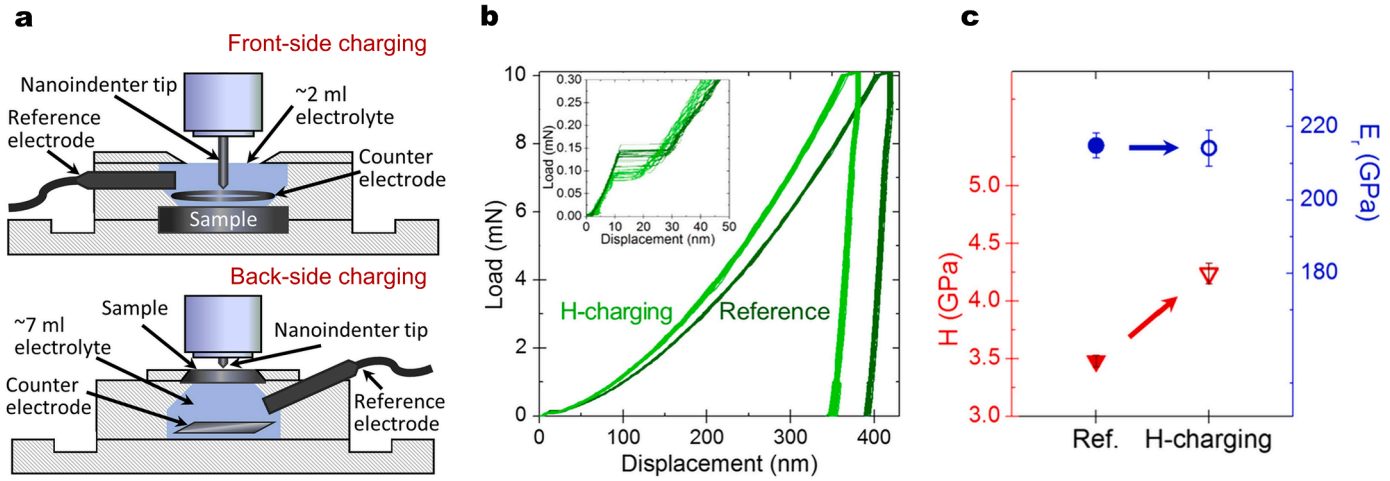

Fig. 3. (a) Schematic diagram of the experimental setup for *in-situ* nanoindentation tests with concurrent H charging implemented by the front-side or back-side charging methods [67]; (b) Representative load-displacement curves and (c) the nano-hardness and elastic modulus values of a Fe-20Cr alloy tested in air and under *in-situ* electrochemical H charging condition [67].

alternative theory claimed that the hardness increased due to a more intensive dislocation-dislocation interactions close to the indents promoted by H-facilitated dislocation nucleation [30,74,75]. As for the H effect on elastic modulus, it is quite slight for BCC alloys with low a H solubility (Fig. 3(c)) [76]. However, due to the high H solubility in FCC structures and the resulting H-related lattice expansion, a decreased elastic modulus caused by H was observed by Lawrence et al. [77] in pure Ni.

Some recent experiments based on advanced ETEM have also brought interesting insights on the interplay between H atoms and dislocations. In contrast to the previous *in-situ* ETEM where a thin foil of materials was loaded monotonically under H atmosphere, Xie et al. [60] have applied cyclic loading on pillar-typed specimens and monitored the forward-and-back motion of dislocations under ETEM (Fig. 4(a)). In single-crystal Al, they observed that all the probed dislocations remained fixed after hydrogenation, which was entirely different from the cyclic, reversible motion of these dislocations loaded in vacuum (Fig. 4(b)). This strongly suggested an increasing effect of H on the critical stress for dislocation gliding, i.e. dislocation locking by the presence of H. However, they found that the required segregation time of H to lock dislocations was much slower than that expected from H lattice diffusion. As such, they attributed such locking effect to the segregation of hydrogenated vacancies to the dislocation core, a more sluggish process than interstitial H diffusion. In a more recent separate work, Xie et al. [78] used the same setup to study the H-dislocation interaction in pure Fe, from which a completely different conclusion was drawn. In that study, H was found to enhance (rather than suppress) the screw dislocation motion in Fe at low H concentrations, showing ~28% reduction of dislocation activation stress and more than 64% enhancement of dislocation bow-out distance. In addition to mass-produced bulk materials, *in-situ* ETEM technique is also a useful tool to understand HE in nano-sized materials. For example, Yin et al. [79] recently performed *in-situ* TEM tensile tests in penta-twinned Ag nanowires to reveal the interplay between H and defects in nanostructures. They demonstrated that H adsorbed at surface could enhance the yield strength and facilitate localized deformation via suppressing the dislocation nucleation at surface. It should be noted that although *in-situ* ETEM can provide unique direct visualization on H-dislocation interactions that help to understand HE, tremendous efforts have to spend on specimen preparation, *in-situ* probing, data interpretation, etc. Advanced expensive facilities are also essentially required, which are not accessible for many research groups in the world. The high expense associated with such

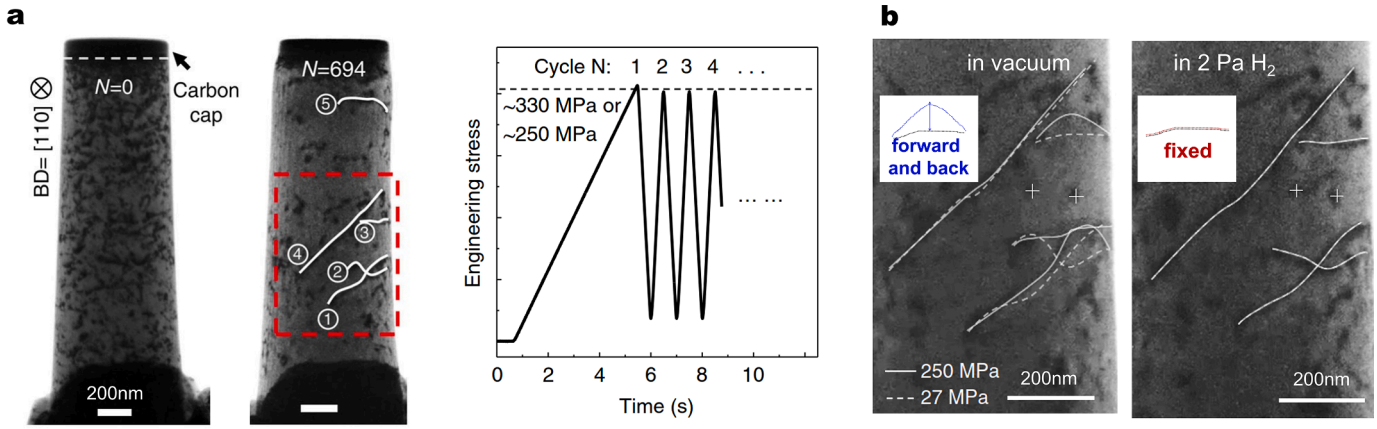

Fig. 4. (a) Microstructure of the pillar-typed specimen before loading in H_2 and the profile of cyclic compression loading used in the work of Xie et al. [60]. The as-fabricated pillar ($N = 0$, left figure) contained a high density of dislocations, which can be mechanically annealed after cyclic compression ($N = 694$, middle figure); (b) The response of dislocations in pure Al to cyclic loading in vacuum (left figure) and after hydrogenation. The insets schematically describes the relative dislocation movement in vacuum (the black dash line signifies the original dislocation position and blue dash line highlights the dislocation position after loading) and in H_2 atmosphere (the black and red dash lines correspond to the dislocation position before and after loading, respectively) [60].

experiments strongly limits the number of experiments that are abundantly needed to identify the operating boundary conditions of various H-associated phenomena, which is one key to fully understand HE in metallic materials.

Hydrogen embrittlement in the fields of hydrogen storage and transport

The development of safe, efficient and cost-effective storage and transport systems and equipment is the key for establishing an economically feasible H-fueled society. H is a lightweight gas and has the lowest volumetric energy density among all kinds of fuels at normal temperature and pressure. As such, one of the most significant challenges for H storage is how to increase the gravimetric and volumetric storage capacity (i.e. storage efficiency) while still maintaining lightweight, compact and safety of equipment. Available options include high-pressure gaseous storage, cryogenic liquid storage and solid storage through metal hydrides and porous structures to physically or chemically absorb H [80]. Among these approaches, high-pressure H_2 storage is the simplest, most established and most efficient storage technologies currently in use for both, mobile and stationary storage systems [80]. There are typically four types (Type I to type IV) of high-pressure H gas vessels or tanks made with different materials. Some detailed information along with some advantages and disadvantages of these pressure vessels are listed in Table 1. Due to the relatively low cost, high load-bearing capacity and the durability of metals, they are widely used in H gas pressure vessels, especially for Type I and Type II vessels as well as for vessel-associated components such as valves, pressure relief devices and fittings [81]. Commonly used metallic materials in this area include Cr-Mo steels, stainless steels and Al alloys (mainly 6061 and 7000 grades). These materials have all shown to be susceptible to HE to some degree. Although some of these materials have been successfully used in gas and petroleum industries with regulated environmental and mechanical conditions, whether they are reliable enough to be used in H energy infrastructures (with potentially a higher H pressure and purity) needs to be carefully assessed. With respect to H transport, pipeline transmission is established as the most economical and efficient method for high-throughput and long-distance transportation [82–84]. Until 2016, over 4500 km pipes have been built around the world (mainly in U.S. and Europe) to transport H [85]. There are also continual discussions on whether the existing natural gas pipeline networks could be used to carry H_2 or H_2-natural gas mixture. The HE sensitivity generally observed in pipeline steels is a key issue to consider. The primary focus of this section is thus to provide a systematic assessment on the HE behavior of metallic materials typically used in H storage and transport, with the objective to aid their wider application in the dawning H energy industry. The H-induced damage behavior and the associated mechanisms of these materials are also briefly covered and discussed.

Hydrogen embrittlement of low-alloy Cr-Mo steels

Low-alloy Cr-Mo steels (e.g. AISI/SAE 41xx grades) are widely used in pressure vessels due to their good combination of strength and toughness and the relatively low cost. These steels typically contain 0.5~1.1 wt.% Cr, up to 1 wt.% Mo and a C level up to 0.6 wt.%. Some microalloying elements such as V and Ti are sometimes also added with the aim to form H-trapping carbides that are potentially beneficial for HE resistance [88,89]. They are normally supplied in quenched and tempered state, thus possessing a primarily tempered martensite microstructure (Fig. 5(a)). Most studies on the HE behavior of these steels have concerned H trapping and H-induced degradation of mechanical properties, with particular focuses on the effects of testing and metallurgical conditions (e.g. composition and microstructure) [88–91]. Both methods of electrochemical charging and high-pressure H_2 gaseous charging have been used in the previous literature to reveal the effects of H. Here we mainly summarize the data acquired from the latter charging method, which should be more relevant to the operating environment in H energy application. Figs. 5(b)~(d) show the effect of H on the tensile properties, fracture toughness and fatigue resistance of some commercial Cr-Mo steels that are loaded under high-pressure H_2 gas [14]. It is demonstrated that H environment has only weak influence on tensile strength but a strong degradation effect on steels' ductility (Fig. 5(b)), fracture toughness (Fig. 5(c)) and fatigue crack growth rate (Fig. 5(d)). It is more interesting to find that only a limited H_2 pressure (1.1 MPa) can already result in a prominent deleterious effect (~2/3 drop in fracture toughness as shown in Fig. 5(c)), and such effect becomes much weaker with further increase in H_2 pressure (e.g. from 1.1 to 10 MPa). Michler et al. [92] also summarized the mechanical property data of a number of steels and observed a similar trend, based on which they proposed the following relation between HE index (HEI) and H fugacity (f): $HEI = mf^n$, where HEI is the ratio of the mechanical property (e.g. reduction in area, total elongation, fracture toughness and crack growth rate) measured in H_2 and in air, and m and n are materials' relevant constants.

Among all characteristics of materials, the strength level, determined largely by the steels' C content and tempering temperature, has the most prominent influence on the HE resistance of Cr-Mo steels. Fig. 6(a) shows that a higher yield strength reduces the fracture toughness at the onset of subcritical crack growth under high-pressure H_2 environment. Such antagonism between strength and HE resistance, generally existed also in other alloys [54], must be carefully considered when designing structural components operated in H-abundant environments. The service environment also affects materials' HE susceptibility [14,94–97]. A particularly interesting finding is that the addition of a small amount of gas impurities (~1 %) within H_2 can strongly influence steels' fatigue crack growth rate up to several folds, as shown in Fig. 6(b) [14]. It is demonstrated that some gas additives like O_2 and CO suppress H-induced fatigue crack growth crack, while some (CH_3SH and H_2S) promote H-induced cracking (Fig. 6(b)). Shang et al. [94] also showed that at a same H_2 partial pressure, the addition of even inert gas like N_2 (thus a higher total pressure) can significantly impact the H-induced cracking behavior. Common explanations attribute these influences to the impact of other gas molecules on the process of H ingress (i.e. rate of H_2 adsorption, dissociation or H surface diffusion [94,96]). These results strongly suggest that the evaluation of H compatibility or HE of a certain material/component must adequately consider the real service environment.

With respect to the behavior of H-induced damage and the associated mechanisms, systematic and in-depth studies for commercial Cr-Mo

Table 1
Detailed information of different types of pressure vessels for H gas storage [86,87].

Type	Structure and materials	Typical Pressure (MPa)	Gravimetric Density (wt.%)	Cost ($/kg)	Advantages	Disadvantages
I	All-metal construction	20	1.7	83	1. Large storage capacity due to the large tank size that can be produced; 2. Cost-efficient.	1. Heavy; 2. Typically low pressure (i.e. low storage efficiency).
II	Load-bearing thick metal liner hoop wrapped by fiber-resin composite	30	2.1	86		
III	Non-load-bearing metal liner fully wrapped by fiber-resin composite	70	4.2	700	1. High storage efficiency; 2. Light.	1. Expensive.
IV	Composite construction with polymer liner	70	5.7	633		

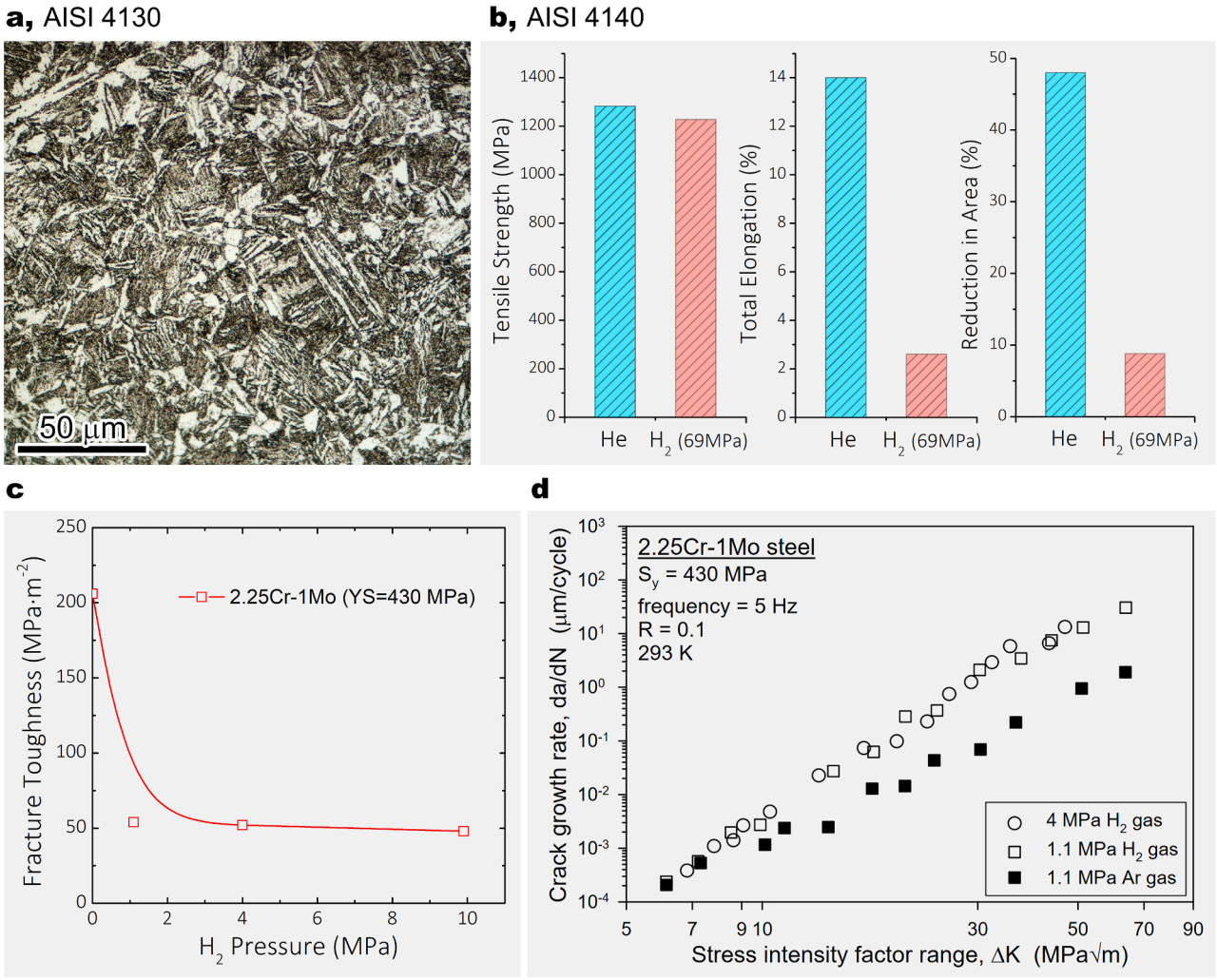

Fig. 5. (a) Optical micrograph of an AISI 4130 steel in as-received state, showing a primary martensite structure with a small fraction of ferrite [93]; (b) Comparison of tensile strength, total elongation and reduction in area between an AISI 4140 steel loaded under 69 MPa He and the same material loaded under 69 MPa H_2 [14]; The influence of H_2 on (c) the fracture toughness and (d) the fatigue crack growth rate of a 2.25Cr-1Mo steel [14].

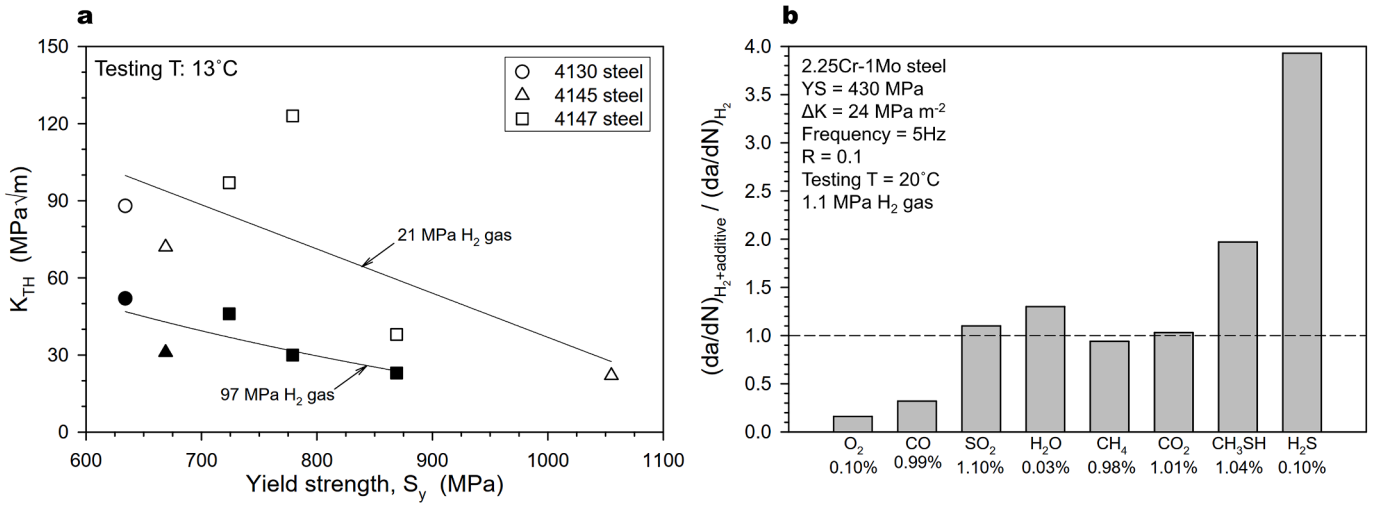

Fig. 6. (a) Influence of yield strength on the fracture toughness at the onset of subcritical crack growth (or threshold stress-intensity factor for crack extension) in Cr-Mo steels tested in high-pressure H_2 gas; (b) Ratio of fatigue crack growth rate measured in H_2 gas with additives to fatigue crack growth rate measured in pure H_2 gas for the 2.25Cr-1Mo steel, showing the influence of the testing environment [14].

steels are still scarce [93], although some insightful work on other types of martensitic steels (e.g. Fe-C binary steels and C-Mn high-strength steels) exists [5,98–101]. Depending on the testing condition (e.g. environment and strain rates), H concentration, microstructure and alloying composition, the fracture surface of H-deteriorated Cr-Mo steels can show either intergranular, cleavage, quasi-cleavage or dimple-typed behavior [102–105]. Liu et al. [104] have studied the HE behavior of a 1.4Cr-1.1Mo-3.2Ni (in wt.%) steel and showed that the fracture surface gradually changed from ductile dimple, to quasi-cleavage and to brittle intergranular fracture with increasing H concentrations that were introduced by electrochemical pre-charging. Recently, Connolly et al. [93] have applied a novel experimental setup combining synchrotron high-energy X-ray diffraction and *in-situ* deformation under 1.7 MPa H_2 gas, in order to study the mechanisms of H-induced fatigue crack growth in a AISI 4130 steel. They observed an enhancement of the elastic strain field near the fatigue crack grown in H_2 compared with that in air, which indicated an increased effective stress-intensity factor due to the presence of H. Such observed was consistent with the transgranular HEDE mechanism. Further, they also found a reduced dislocation density at near-crack regions for the sample loaded in H_2. This behavior was attributed to the HELP mechanism in terms of the H-facilitated movement of dislocations from grain interiors to grain boundaries, which subsequently resulted in intergranular HEDE. A promoted transgranular crack growth due to HEDE and the H-induced intergranular cracking due to HELP facilitated HEDE were thus concluded as the key mechanism for the more rapid fatigue crack growth observed when samples were loaded in H_2 environment. There is no doubt that such experiments provide new insights on the operating HE mechanisms in Cr-Mo steels. However, whether the proposed mechanisms are universal for other Cr-Mo steels with different testing and materials' conditions remains a question and requires further studies.

Hydrogen embrittlement of pipeline steels

Due to the low alloying contents, pipeline steels also possess a ferritic matrix. Depending on the specific thermomechanical processing routes, the microstructure can consist of one or more phase constituents including pearlite, polygonal ferrite, quasi-polygonal ferrite, Widmanstätten ferrite, acicular ferrite, bainitic ferrite, bainite and martensite [106]. The microstructure ingredients largely determine the

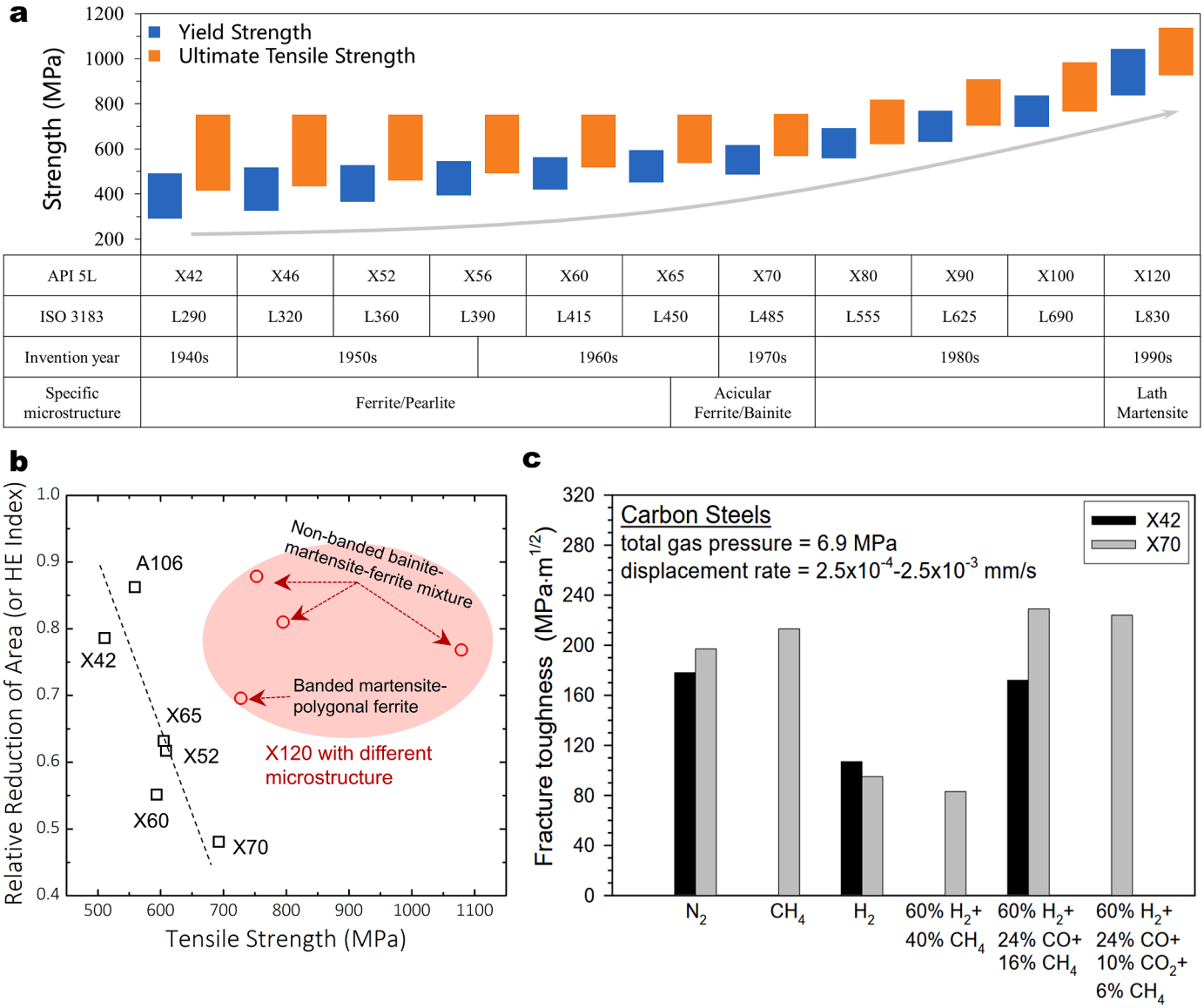

Fig. 7. (a) Evolution of pipeline steels with time [84]; (b) The relative reduction of area (or HE index) of some pipeline steels tested in ~7 MPa H_2 and air [8,14]; (c) Influence of gas composition on the fracture toughness of X42 and X70 steels [14].

strength of the steels. Fig. 7(a) provides a brief overview on the evolution of pipeline steels including their strength levels and the associated microstructural states. An enhanced strength level is achieved for more advanced pipeline steel grades. In general, similar to Cr-Mo steels, an increased strength tends to reduce the HE resistance of pipeline steels for a similar microstructural and testing condition (see data of X42~X70 in Fig. 7(b)). The specific microstructure also poses a substantial influence on the HE behavior. For example, Villalobos et al. [8] have studied the tensile property a X120 steel with different microstructural states exposed to high-pressure H_2 gas. Related data are also plotted in Fig. 7 (b). It is shown that the sample consisted of a banded martensite-polygonal ferrite microstructure had the lowest HE resistance among all the studied materials, despite the lower strength of this sample. It is generally predicted that prior to carrying pure H_2, steel pipelines will be used to transport mixed gas (e.g. H_2 and natural gas mixtures) in the shorter term [84]. The influence of gas composition or impurity on the HE response is thus important to be evaluated. Fig. 7(c) provides some data in this aspect [14]. It is interesting to find that the fracture toughness of two pipeline steels (X42 and X70) is lower under H_2 and CH_4 mixed gas compared to the value under pure H_2, whereas the addition of some gases such as CO or CO_2 to the testing environment seems to eliminate the H degradation effect. The underlying reasons might be associated with the different surface absorption behavior of molecular H_2 from the different atmosphere, which affects the kinetics of H ingress into steels' lattice [107,108]. Other factors (e.g. H concentration and H_2 pressure) influencing the HE response in pipeline steels have been thoroughly summarized in Ref. [14] and will not be covered here.

Due to the complex and highly variable microstructure of pipeline steels, controversial observations and opinions with respect to the H-induced damage features and the underlying mechanisms have been raised. Martin et al. [109] have observed some typical "flat" featureless regions on the fracture surface of a X60 pipeline steel deformed under high-pressure H_2 gas (Fig. 8(a)). These regions, when probed by high-resolution and topological characterization techniques, reveal dense undulations and small (~50 nm) rounded mounds (Fig. 8(b)). They proposed that these undulations and mounds were formed due to either near-surface relaxations associated with formation of new surfaces or to the decohesion at weak regions associated with the H-enhanced dislocation activity and local high H concentration (Fig. 8 (c)). Similar fracture features have also been observed by Neeraj et al. [6] in similar pipeline steels, as shown in Figs. 8(d) and (e). They have further demonstrated that these fine features on the "brittle" facets appeared to be "valley-on-valley" type, rather than "mound-on-valley" type that can be inferred from the argument of Martin et al. [109]. Therefore, they proposed that these features were more likely to be nano-dimples that were formed due to H-enhanced super-abundant vacancies and the subsequent vacancy agglomeration (schematically shown in Fig. 8(f)) [6].

In addition to the above-mentioned quasi-cleavage typed fracture surface with undulated facets, some other fracture behavior has also been reported in pipeline steels loaded in the presence of H, which are exemplified in Fig. 9 [109–111]. Martin et al. [109,112] have identified distinct ridges decorated with saw-teeth features on the cleavage fracture of the same sample shown in Figs. 8(a) and (b). They believed that these features are the consequence of H-enhanced slip band formation (fully consistent with the HELP model) and H-assisted void nucleation and evolution. In contrast, Hattori et al. [110] have investigated the HE behavior of a X80 steel and found that both the H pre-charged and non-charged specimens were fractured in a ductile manner (with well-developed dimples shown in Figs. 9(c) and (d)), although the H-charged specimen exhibited a significant ductility loss. The only difference was that the dimples in the H-charged specimen appeared to be shallower than the H-free counterpart and their nucleation was not associated with inclusions or second phase particles (Figs. 9(c) and (d)). They attributed such fracture phenomenon to the promoting effect of H on the formation of vacancies and vacancy clusters [110]. In other scenarios, it is also found that the presence of H can promote decohesion between inclusions and matrix (Fig. 9(e)), regardless of whether deformation is applied or not [9,109,111], which suggests the HEDE mechanism might play a role here. The above brief overview demonstrates that a highly variable nature of the H-induced damage and fracture behavior in pipeline steels. The activation of specific HE mechanism should be dependent on its microstructure-relevant boundary condition and the performed testing conditions.

Hydrogen embrittlement of stainless steels

The most widely used stainless steels in the field of H_2 storage are austenitic stainless steels. These steels generally possess a higher HE resistance compared with ferritic and duplex stainless steels, with one important reason being the slower H diffusivity inside austenite. The

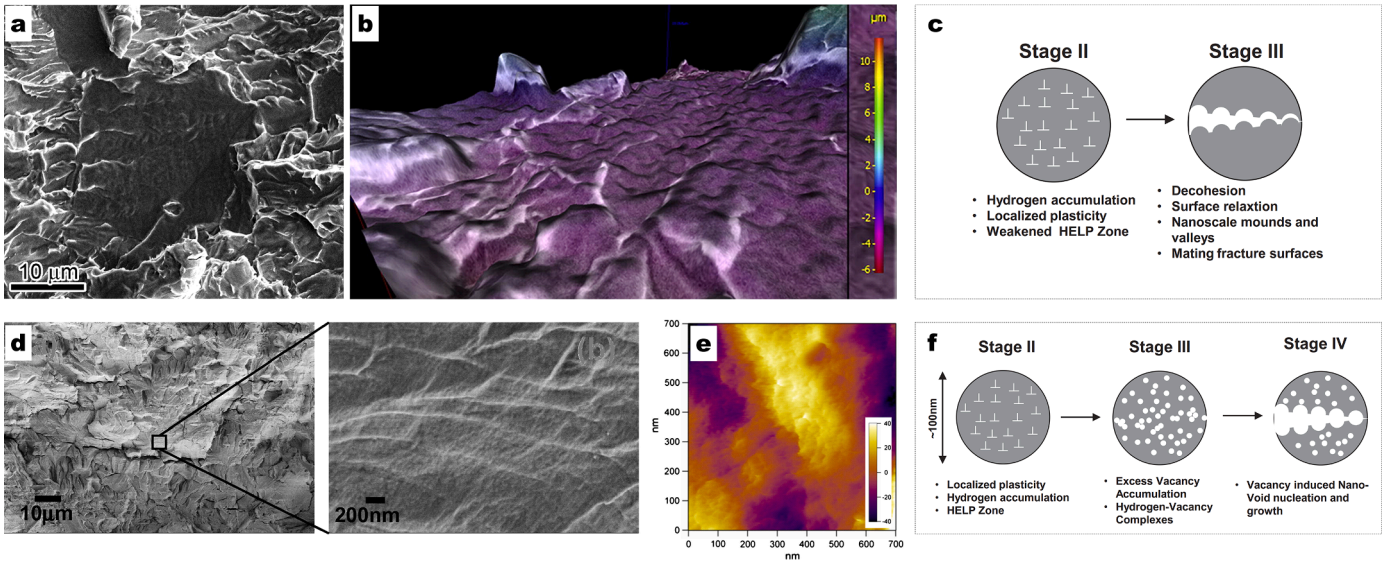

Fig. 8. SEM observation of the fracture surface of (a) X60 pipeline steel deformed under high-pressure H_2 gas [109] and (d) X65 pipeline steel that was H pre-charged and deformed to fracture [6]; (b) Topological image of the "flat" facet in (a) [109]; (e) Atomic force microscopy (AFM) image from a quasi-brittle facet of the same fractured specimen in (d) [6]; (c) and (f) are proposed mechanisms accounting for the undulations or nano-dimples observed in (b) and (e), respectively [6].

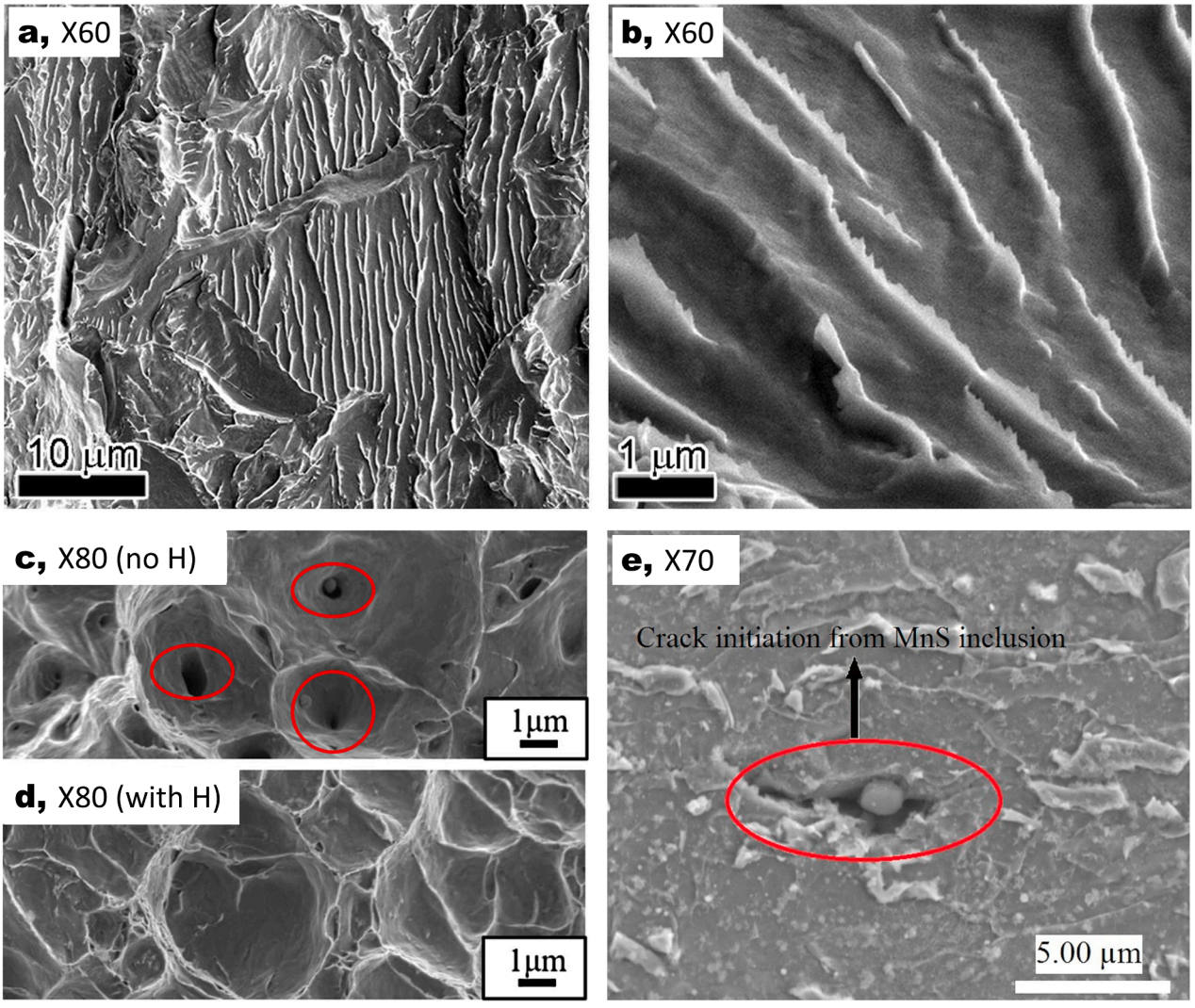

Fig. 9. Different H-induced fracture/cracking features that have been observed in typical pipeline steels. (a) quasi-cleavage fracture behavior with striations or ridges in a X60 steel loaded under H [112]; (b) high-magnification image showing ridges with saw-teeth features; Dimple typed fracture behavior of a X80 steel loaded (c) without H and (d) after H pre-charging [110]; (e) Crack initiation at the inclusion-matrix interface induced by H charging [111].

reported H diffusion coefficient inside austenite is typically more than 3 orders of magnitude lower than that in ferrite at room temperature [113]. The HE susceptibility of austenitic stainless steels is critically dependent on the composition and the associated austenite mechanical stability against deformation-induced martensite transformation [114,115]. A higher Ni content in these steels favors a higher HE resistance at both relatively low temperature (−50 °C) and room temperature, regardless of when and how H is introduced (Figs. 10(a) and (b) [116]). Such effect of Ni can be attributed to its enhancing role in stabilizing austenite and thus in reducing the amount of deformation-induced martensite formation upon loading. The relation between HE response and austenite stability can be better correlated by plotting the HE index (relative reduction of area, RRA) as a function of Md_{30} temperature (as shown in Figs. 10(c) and (d) [115]). This temperature, defined by the temperature point at which half of the austenite is transformed to martensite after a strain of 30 %, is usually used to quantify the mechanical stability of austenite [7,117,118]. Based on Figs. 10(c) and (d), Izawa et al. [115] concluded that the HE sensitivity of low-Ni austenitic stainless steels, determined by comparing the reduction of area of samples loaded under high-pressure H_2 and under reference atmosphere (air, Ar or N_2), can be separated into three regimes: a) for Md_{30} above −80 °C, the HE susceptibility reduces with increasing austenite mechanical stability (lower Md_{30} temperature); (b) for Md_{30} around −80 °C, the HE susceptibility shows a large variation among the literature; (c) for Md_{30} below −80 °C, the steels are resistant to HE when they are tested under high-pressure H_2 (results can be different in other testing scenarios, see blue points in Fig. 10(d) and figure caption). Note that the Md_{30} temperature in the study of Izawa et al. [115] was calculated using the empirical equation proposed by Nohara et al. [119]. Other equations might result in different Md_{30} values, but the above proposed general trend regarding the correlation between Md_{30} the HE susceptibility will not be changed. In addition, some deviated data points can also be found in Figs. 10(c) and (d) (marked by a circular frame). Such deviation might be associated with the influence of sample surface condition, macro-segregation and metallurgical impurities that might vary among different samples and studies [115].

The detrimental influence of deformation-induced martensite (especially α'-martensite with a body-centered tetragonal structure) on HE resistance of steels can be understood by the following two aspects: Firstly, the formation of deformation-induced martensite raises the local stress which increases the driving force for crack formation and favors stress-driven H migration. The diffusion and accumulation of H inside the microstructure to regions of high local stress is considered as one of the main reasons for HE [20], regardless of the prevalent mechanisms.

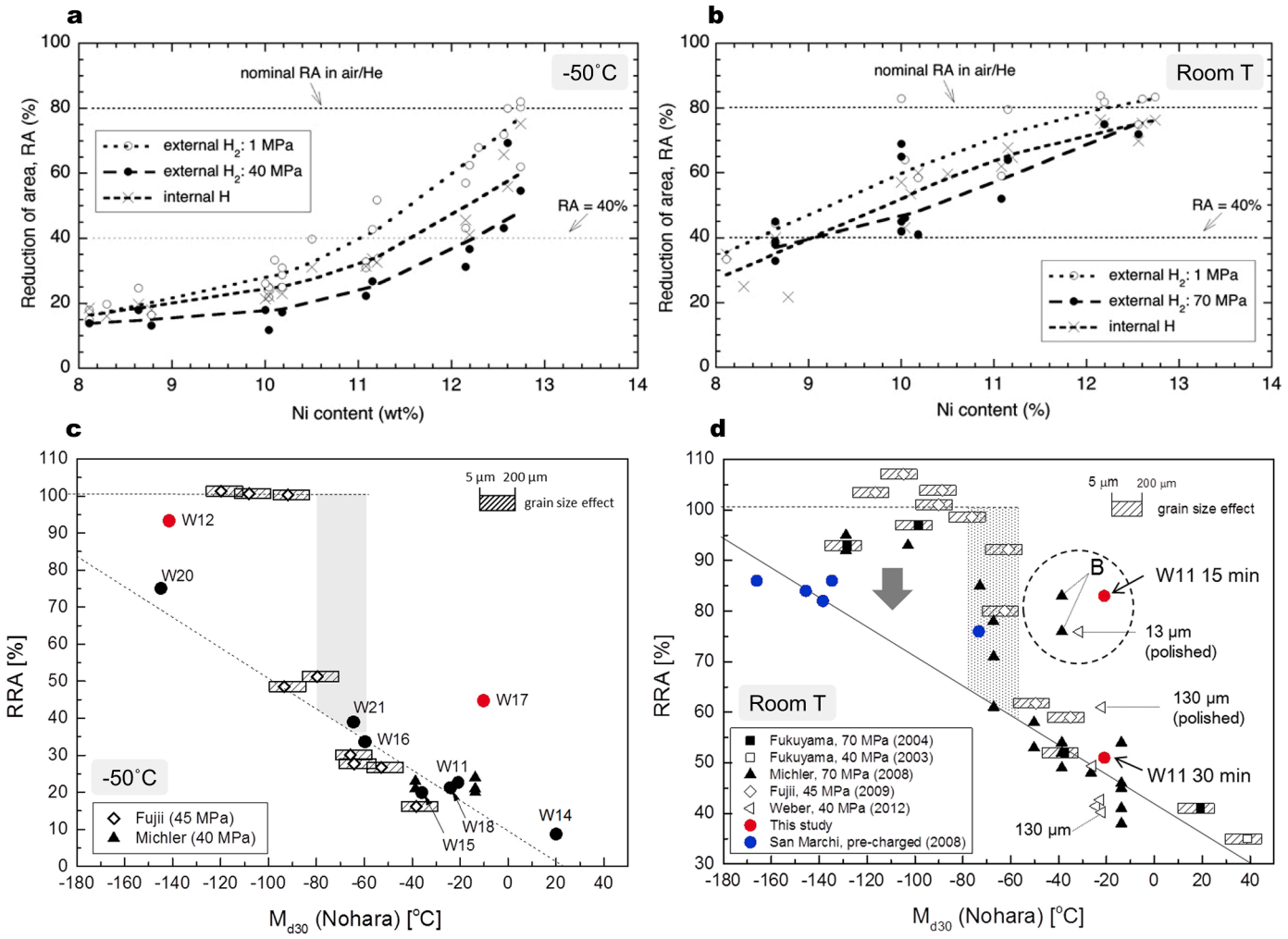

Fig. 10. Effect of Ni content on the reduction of area of austenitic stainless steels deformed with the presence of H at (a) −50 °C and (b) room temperature [116]; Correlation between relative reduction of area (RRA or HE index) and Md_{30} temperature for various austenitic stainless steels tested at (c) −50 °C and (d) room temperature [115]. Different codes (W11~W21) in (c) and (d) represent different austenitic stainless steels with different composition. The blue dots in (d) were from samples that were thermally pre-charged to reach a saturated and uniform distribution of H. These samples showed more severe HE than those undergone *in-situ* H_2 gas charging (black symbols in (d)).

Also compared with austenite, α'-martensite is a less tough phase that is more susceptible to HE. Secondly, the host phase (austenite) possesses a higher solubility and lower diffusivity of H compared with the product phase (α'-martensite), differing both by more than two orders of magnitude [120,121]. Thus, the dynamic transformation converts the H atoms from their initial low-mobility solute state in the host phase to a super-saturated and highly mobile state inside the product phase (as schematically shown in Fig. 11(a)) [120,122,123]. The following rapid interaction between the super-saturated H and various types of lattice defects (e.g. vacancies, dislocations and interfaces) then promotes damage nucleation and propagation [20,124]. This latter point can be supported by the existence of martensite phase that is frequently observed surrounding the propagating H-induced cracks in steels containing metastable austenite (Figs. 11(b) and (c)) [7,54,125].

For stable austenitic stainless steels, HE can still occur under harsh conditions (e.g. a higher H concentration or lower testing temperature), although the influence of H is weaker in these steels compared with that in metastable ones [126]. The fracture surface of these steels loaded with the presence of H can show dimple-typed [126,27], quasi-cleavage [127–129] or intergranular [127,128] fracture behavior, depending on the materials' characteristics and testing conditions. Michler et al. [126] have compared the HE response of a series of stable austenitic steels and pointed out the gliding mode of dislocations (cross slip or planar slip) was also an important factor influencing steels' HE resistance. In principle, dislocation planar slip would result in a more heterogeneous or localized stress distribution, especially at the intersections between slip bands and at dislocation gliding obstacles (e.g. other different oriented slip bands and interfaces). The high stress concentration and the promoted H aggregation in combination lead to facile formation of H-induced damage. The frequent dislocation cross slip, on the other hand, can release local stress concentrations and give rise to a more homogeneous stress field, a factor that can reduce the tendency of damage formation. In some other literature (e.g. Ref. [130]), it has been reported that H can increase the slip planarity of dislocations, which could be another factor favoring H-induced damage in austenitic stainless steels (with reasons mentioned above).

Hydrogen embrittlement of Al alloys

The HE behavior in Al alloys has been systematically discussed in recent reviews, (e.g. Ref. [131]), here we only contemplate on some important points relevant to H ingress, trapping and some recent progress in the understanding of HE mechanisms in Al alloys. Available data suggest that the mechanical properties of Al alloys are not affected by gaseous H_2 if moisture is absent. This is because Al_2O_3 are readily formed on the surface of Al alloys and such oxide layer does not

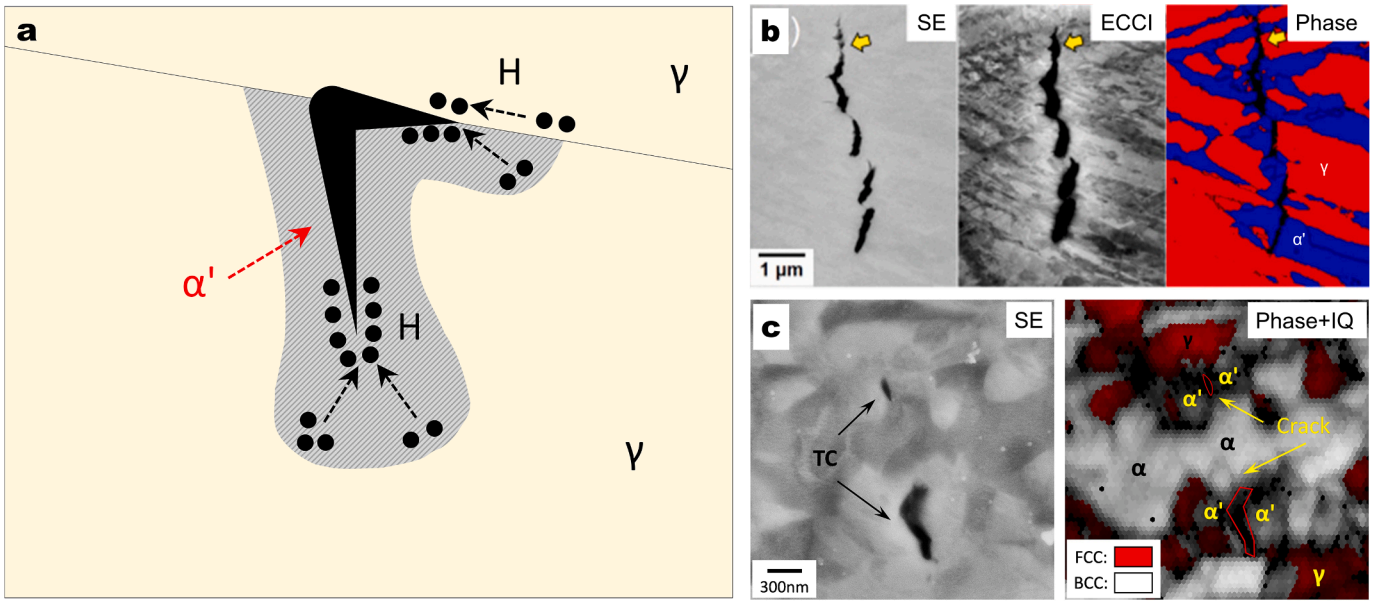

Fig. 11. (a) Schematic diagram showing the influence of deformation-induced martensite transformation on H migration and crack propagation; Typical H-induced micro-cracks and the surrounding microstructure in (b) a AISI 304 stainless steel [125] and (b) a medium Mn steel containing ferrite and metastable austenite [54] (ECCI: electron channeling contrast image, IQ: image quality map).

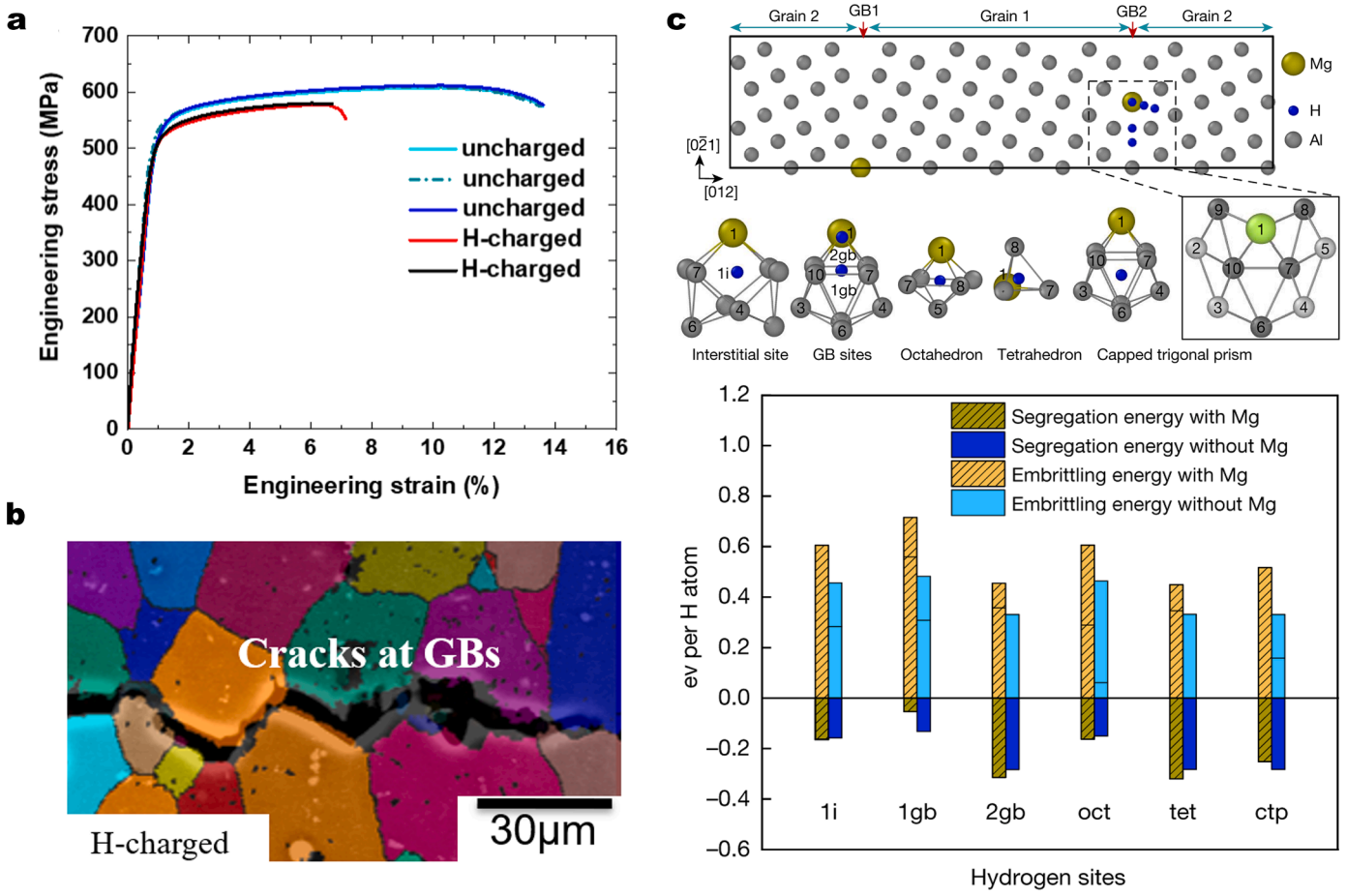

Fig. 12. HE phenomenon and associated mechanisms in a peak aged 7xxx Al alloy: (a) Engineering stress-strain curves of samples in the uncharged and electrochemically H-charged condition [15]; (b) EBSD phase plus IPF showing the H-induced crack along grain boundaries; (c) Density functional theory (DFT) calculations showing the embrittling behavior of H and its interplay with Mg atoms located at grain boundaries [15].

dissociatively chemisorb atomic H when exposed to H_2 gas. HE in Al alloys thus mainly occurs in the presence of water or atomized H_2 which provides favorable condition for continuous H ingress. Although solid Al alloys have a lower solubility in their perfect lattice as opposed to other FCC materials, Al is highly reactive with water which can produce a high fugacity H gas [132]. This reaction is thermodynamically favorable [131]. Furthermore, Al alloys can absorb H when they are heat treated, e.g. during homogenization, as well as in service when exposed to aggressive environments or during corrosion as a result of the destruction of surface oxide layer [133,134].

The solubility of H in Al is low in a perfect solid Al lattice [131], while H has a higher solubility in liquid Al. Such large difference can lead to the formation of porosity, which influences the fatigue properties in cast Al alloys. Alloying elements and microstructural defects can influence the H solubility of Al alloys. The addition of Mg and Li is known to increase the solubility of H in both solid and liquid Al due to their pronounced affinities for H atoms [135]. Cu, Si and Zn, on the other hand, increase the H solubility only in solid Al due to the second-phase trapping effect, while having no effect on the liquid solubility of H. Temperature, alloy compositions, and microstructural defects also influence the diffusivity of H in Al alloys [131,136]. The dissolved H atoms can be trapped and segregated at various trapping sites in Al alloys, such as vacancies, dislocations and grain boundaries, which considerably influences the alloys' mechanical properties. The trapping behavior of H at second-phase particles has been shown by Su et al. [137,138] using high-resolution X-ray tomography and the 4-dimensional strain mapping. A recent study showed that H led to a significant drop in the ductility of Al-Zn-Mg-Cu alloys, with the crack formation along grain boundaries as shown in Fig. 12 [15]. Using the cryo-transfer atom probe tomography, the authors showed that H can be trapped at second-phase particles (e.g. Al_3Zr) and grain boundaries [15]. The H-induced intergranular cracking was explained by the H trapping and its interplay with the preceding Mg decoration at grain boundaries [15,139,140]. The strong trapping of H into the second-phase particles might also pose a beneficial effect on HE resistance of Al alloys. For example, Wang et al. [141] introduced the T phase in a high-strength Al-Zn-Mg-Cu alloy and demonstrated an improved HE resistance due to the H trapping effect of this second phase.

The HELP effect has also been regarded as one mechanism for H-induced damage in Al alloys. Bond et al. [59] have studied the effect of H on the deformation behavior and the fracture process of high-strength Al-Zn-Mg-Cu alloys and concluded that H enhanced the dislocation motion. Albrecht et al. [142,143] also demonstrated that the intergranular fracture of commercial 7075 Al-Zn-Mg-Cu alloys was caused by the dislocation-driven H migration to grain boundaries. In addition, the interaction between H and vacancies can play a crucial role in HE in Al alloys as well. First-principles studies on the formation and thermodynamic stability of H-vacancy complexes showed that H can be significantly trapped at vacancies [132,144,145]. Such process might strongly decrease the mobility of dislocations, as shown from the work of Xie et al. (Fig. 4) [60]. The formation of hydrides was also sometimes reported in Al alloys, which accounts for the degraded mechanical properties. The hydride Al_3H was found to have a small negative formation enthalpy relative to the energy state of H-free FCC Al matrix [146–148]. The formation of a brittle hydride with the composition of $AlLiH_4$ was observed in a Al-Li alloy, which has been shown to initiate the formation of cracks [149].

Hydrogen attack in polymer materials

In addition to metallic materials, polymer materials are also used in newly developed high-pressure H_2 tanks (Type IV), usually as the liner material. The two main polymer materials used in this area are high-density polyethylene (HDPE) and polyamide (PA) [150]. Unlike metallic materials whose mechanical properties can be degraded by H, the mechanical property of polymers is generally not affected by H [151–154], that is, H-induced embrittlement is not likely to occur in these materials. However, some other problems can occur when these materials are subjected to high-pressure H_2 gas. One of the main concerns about polymer liners is their permeability to H, which may induce critical leakages of gaseous H_2. When H enters such materials and reaches a saturation, a thermodynamic equilibrium state is achieved. A sudden decompression would thus promote the formation of cavities inside the polymer materials, which induces the so-called explosive decompression failure (XDF) [155]. During the rapid gas decompression (RGD) of the H_2 vessels, the dissolved H_2 gas tends to expand and emit from the liner material, resulting in micro-cavitation at the material level of the liner and local blistering failure [155–158] (as demonstrated in Figs. 13(a) and (b)). High-pressure H_2 penetrating the interface between the liner and fiber composites (for Type IV H_2 vessels) can cause liner deformation and collapse during rapid decompression [150,159]. Fig. 13(a) shows such collapse phenomenon and the associated mechanisms [159].

In addition to the polymer liner in high-pressure H_2 vessels, the sealing parts also have risks to fail under high-pressure H_2. Propylene-diene monomer (EPDM) and nitrile-butadiene rubber (NBR) are two polymers widely adopted for threaded connectors sealing in high pressure H_2 environment. These materials can also suffer from blistering with similar mechanisms described in Fig. 13(b). It is important to mention that rubber materials generally have a higher expansion coefficient and H_2 permeability than plastic materials, which will cause more serious blistering during decompression [162]. In addition to H-induced blistering, O-rings can also be failed due to extrusion. The extrusion fracture was caused by a remarkable increase in the volume of the O-rings by swelling, which has been observed at a H_2 pressure above 35 MPa [163]. The damage of the O-rings typically become more serious with an increase in H_2 pressure and temperature and a decrease in the testing frequency [163,164]. One additional risk for polymer materials is the increased temperature which can be caused by a fast H_2 charging rate and sudden collision [150]. Such temperature change may cause thermal instability and thermal aging simultaneously, which will lead to a decrease of mechanical properties [150,152–154]. This is particularly true when the temperature exceeds the glass transition temperature.

Hydrogen embrittlement in the fields of hydrogen energy applications

Currently, H is mainly used as a component or catalyst in ammonia production, oil refining and methanol production. In those fields, H-induced damage phenomena (more commonly referred to high-temperature H attack, HTHA [165,166]) have been widely investigated, particularly in low-alloy steels that are used in these applications. The underlying micromechanisms and the associated technical standards have been well established (see, for example, API RP 941 standard) [165]. Further development of the H production-transport-storage chain is expected to widen H application to a variety of other fields such as power generation and grid balancing, transportation, construction and industries. Unlike service scenarios in gaseous H_2 storage and transport in which most components are operated near room temperature, components in the fields of H energy applications can be subjected to a wide range of exposure temperatures. Extreme examples are rocket and aircraft engines that currently use or plan to use liquid H_2 as the fuel. The service temperature of materials used in these applications can span from −253 °C (for parts used in liquid H_2 tanks or tubes) to more than ~2000 °C (for parts in combustors or burners) [167,168]. A proper assessment of the H-induced damage behavior for metallic materials at non-ambient temperatures is thus also required, which is the focus of this section.

Hydrogen-induced damage at elevated temperatures

Given that the HTHA behavior of low-alloy steels used in the

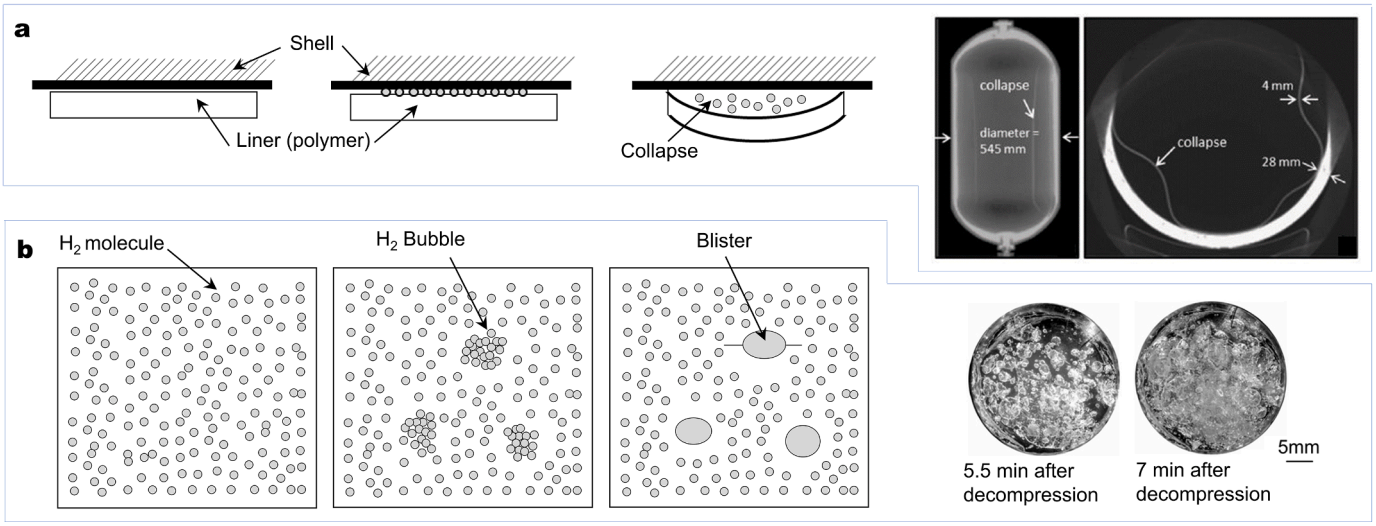

Fig. 13. Phenomenon and associated mechanisms of (a) liner collapse during rapid gas decompression of high-pressure H_2 vessels [159] and (b) blister formation in polymer materials (the images on the right side in (b) are from ethylene propylene diene monomer rubber subjected to high-pressure H_2 decompression) [160,161].

petrochemical industry has been thoroughly reviewed in recent publications [165,166], here we mainly contemplate the H-induced damage phenomenon in high-performance superalloys that are backbone materials in fields of power and aerospace. It is well established experimentally that the degradation effect of H on alloys' mechanical properties is highly dependent on temperature. Generally a maximum

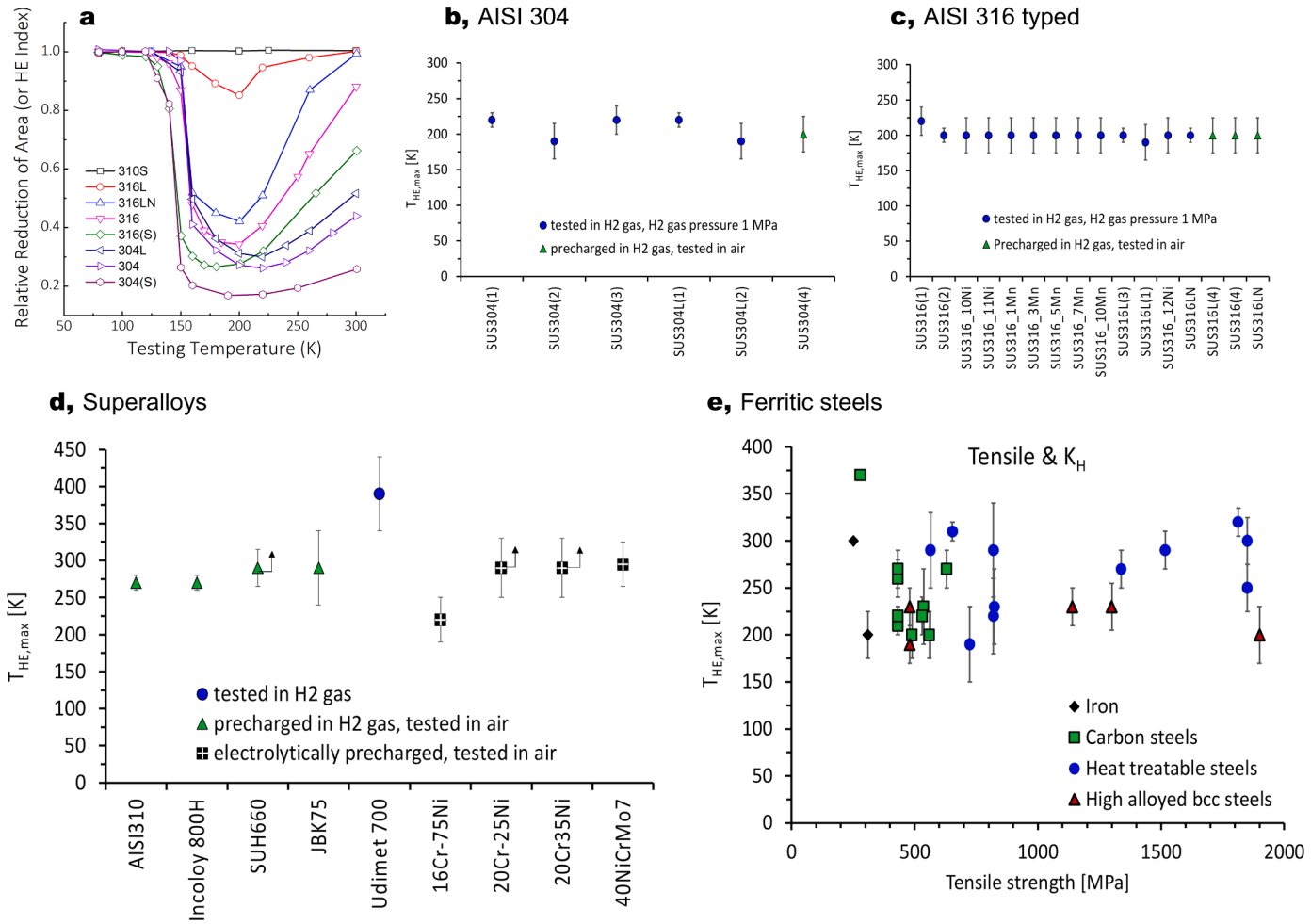

Fig. 14. (a) Influence of testing temperature on the relative reduction of area of type 316 and 304 series stainless steels tested at 1.1 MPa H_2 and He (304 (S) and 316 (S) are sensitized 304 and 316 steels) [175]; The determined value of $T_{HE,\ max}$ for (b) AISI 304, (b) AISI 316, (c) iron- and nickel-based superalloys and (d) ferritic steels (more detailed materials and testing information in these datasets can be found in Ref. [169]).

degradation occurs at a certain temperature ($T_{HE,\ max}$, defined in Ref. [169]), below or above which the deterioration is weaker. Typical examples for some austenitic steels are shown in Fig. 14(a). Michler et al. [169] have collected and analyzed HE testing datasets from ~50 references and reported a $T_{HE,\ max}$ value of around −68 °C, 13 °C and −98 °C~72 °C for some austenitic stainless steels (mainly AISI 304 and 316 and their alloy adjusting variants), iron- and nickel-based superalloys and ferritic steels, respectively (Fig. 14(b)~(e)). This seems to mean that the HE problem for many commonly used materials is most serious close to room temperature (within ±100 °C deviation) and the HE at high temperatures (above 100 °C) is a less concerned problem. However, it should be noted that current investigations about HE at high temperatures are still quite limited. The quantity of testing data and the number of materials that have been studied in the available literature about high-temperature HE are too small to be conclusive. The temperature dependence of HE sensitivity is strongly influenced by the type of materials and their microstructure conditions [168,169]. It is thus likely that some materials (such as some Ni-based superalloys) suffer more from HE at increased temperatures [16,170]. For example, results have showed that Ni-based superalloys EP99 and EP741 experienced a more severe HE at around 500 °C compared with that at room temperature (Fig. 15(a)) [16]. For these alloys, similar to the behavior at ambient temperature, their strength determined from smooth (unnotched) tensile specimens is not significantly influenced by H at elevated temperatures [171,172]. Instead, H possesses a stronger degradation effect on tensile ductility (or reduction of area), notch tensile strength and fracture toughness [171,172]. To give an example, the total elongation of Udimet 700 determined from smooth specimens in H_2 was only about 3 % at testing temperatures ranging from 23 to 680 °C, which was much smaller than the determined value in air (~20 % at this temperature range) [173]. However, it is important to note that specimens tested at high temperature H environment seldomly show a true brittle fracture surface, despite the reduced macroscopic ductility [174]. Instead in most cases, a predominantly dimple-typed fracture, driven by micro-void formation and coalescence, is observed, which is similar to the counterpart samples loaded at the same temperature without H [172,174].

The fatigue properties of some selected superalloys loaded under high-temperature H environment were reported by Harris and Vanwanderham [171]. Some of their results were collected and replotted in Figs. 15(b) and (c). It is interesting to find that, for the Inconel 718 alloy whose tensile ductility is less influenced by H at increased temperatures (Fig. 15(a)), its high-cycle fatigue property is strongly degraded under high-temperature H environment, with a similar degradation degree as that at room temperature (Fig. 15(b)). However, this is not true for its strain-controlled low-cycle fatigue property which is only marginally affected by H at the same temperature (678 °C, Fig. 15(c)). This suggests that for each material, the high-temperature HE susceptibility is highly dependent on the loading scenarios. Further, the H degradation effect on high-temperature fatigue properties is also strongly influenced by the type of materials. For the stress-controlled high-cycle fatigue property, the Inconel 718 alloy was more influenced by H compared with the

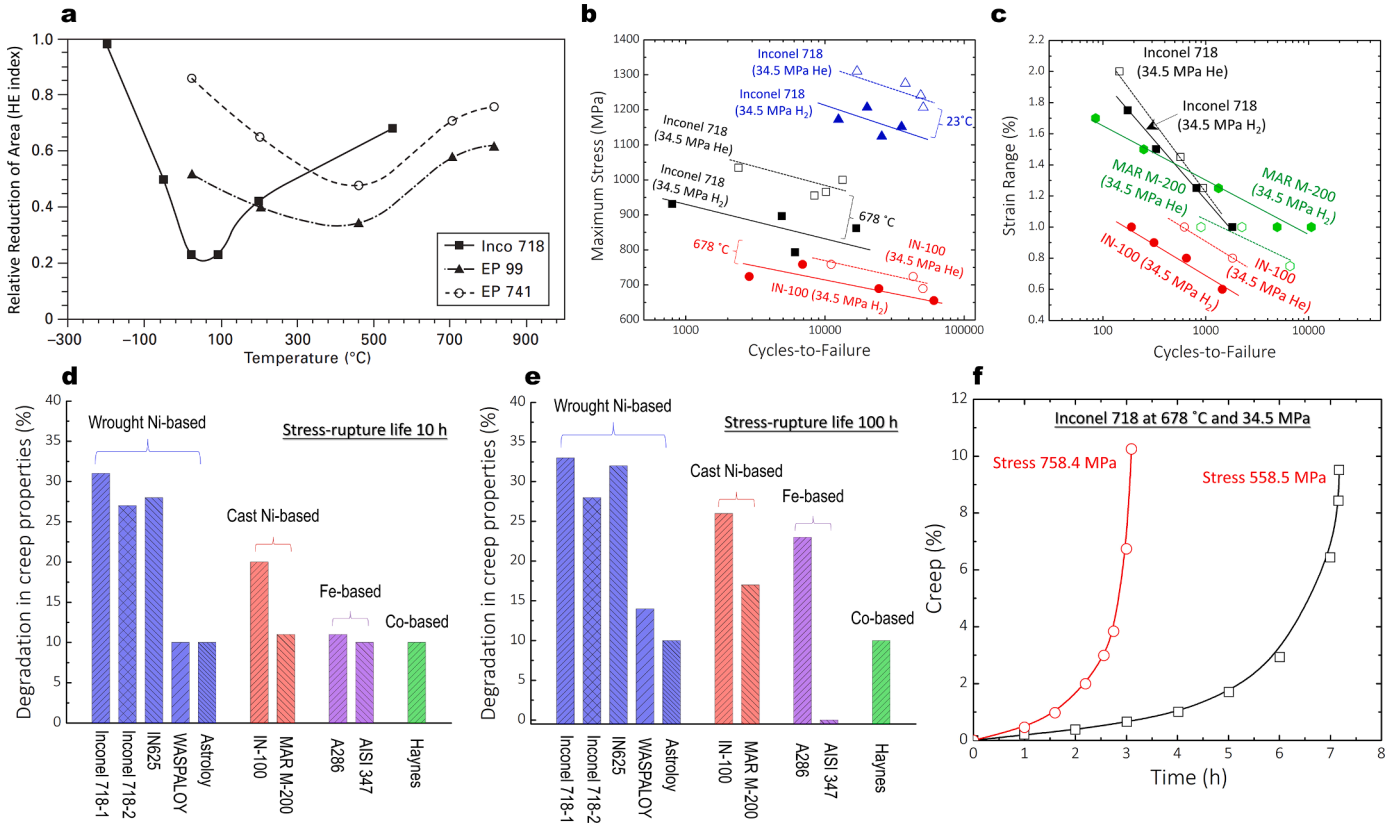

Fig. 15. (a) Influence of testing temperature on the HE index of some Ni-based superalloys. The HE index is here characterized by the ratio of reduction of area between the samples loaded under H_2 and He at the same pressure [16,168,170]. The applied gas pressure is 51.7 MPa for the Inconel 718 sample [168] and is 45 MPa for the EP 99 and EP 741 samples [170] whose data are shown in this figure; (b) Stress-controlled high-cycle fatigue (stress ratio 0.1) property of some Ni-based superalloys tested under 34.5 MPa H_2 and He at different temperatures [171]; (c) Strain-controlled low-cycle fatigue property of some Ni-based superalloys tested under 34.5 MPa H_2 and He at 678 °C [171]; H-induced creep strength degradation of different types of superalloys for a stress-rupture life of (d) 10 h and (e) 100 h (all data shown in these two figures were acquired from creep tests conducted at 678 °C and 34.5 MPa H_2 or He gas. Inconel 718–1 and 718–2 correspond to two different microstructural states adjusted by different heat treatments. Specific values for a degradation level below 10 % is not given in the literature, thus here we assign the upper bound, 10 %, for relevant alloys) [44]; (f) Total creep strain as a function of time for the Inconel 718 alloy tested at 678 °C and 34.5 MPa H_2 or He gas.

IN-100 alloy (Fig. 15(b)), whereas the trend is overturned for the strain-controlled low-cycle fatigue property (Fig. 15(c)). For some superalloys such as the MAR M-200 Ni-based alloy, the presence of H even possessed a beneficial effect on low-cycle fatigue property, although the underlying mechanisms were not understood. Given that the published data regarding mechanical properties under high-temperature H environment are currently very limited, no concluding remarks on the relations between alloy conditions, testing parameters and HE susceptibility can be established.

For metallic materials used in high-temperature applications, one important design property is the creep resistance over extended periods of time. Harris and Vanwanderham [171] have reported the influence of high-temperature H environment on creep properties for a series of superalloys including four wrought Ni-based alloys (Inconel 718, Inconel 625, WASPALOY and Astroloy), two cast Ni-based alloys (In-100 and MAR M-200), two wrought Fe-based alloys (A286 and AISI 347), two wrought Ti-based alloys (Ti 6–4, A-110 and one wrought Co-based alloy (Haynes 188). The creep degradation level was determined from the percentage reduction in stress for the H_2 environment, in comparison to the He environment, to obtain a given stress-rupture life. The testing results conducted at 678 °C and 34.5 MPa gas pressure are summarized in Fig. 15(d). It is demonstrated that the creep property of Ni-based superalloys is generally more sensitive to H compared with that of Fe- and Co-based alloys. Most of the investigated Ni-based alloys have a degradation level between 10 and 35 % under H_2 environment, in comparison to the samples tested at He gas. Lee [16] has proposed that if a certain alloy suffers from HE near the vicinity of room temperature, then it is likely that its creep property will be affected by H at high temperature. If this is a general trend, then the creep resistance of high-temperature materials must be carefully considered and evaluated when applied in H_2 environment.

Pertaining to the underlying mechanisms for the above-mentioned HE phenomena at elevated temperatures, no detailed study and discussion have been reported so far, to the best of authors' knowledge. Speculations have occasionally been proposed though. A few researchers argued that the mechanism is similar to the underlying reason for high-temperature H attack (HTHA) that was commonly observed in steels used in oil, gas and petrochemical industries [16]. That is, the H-induced degradation of high-temperature mechanical properties is due to certain chemical reactions between H and solutes/constituents/impurities in alloys (often C or carbides in steels) and the resulting occurrence of internal cavitation along grain boundaries [16,165]. He et al. [176] have studied the creep behavior of a solution-treated 304 stainless steel under 9.9 MPa H_2 at 550 °C, and they proposed that the reduced creep strength by H was due to the H-induced change of carbide morphology dynamically precipitated at grain boundaries. The formation of hydrides at high temperatures has also sometimes been proposed to explain the high-temperature HE in specific metallic materials (e.g. Nb and Ti alloys) [177,178]. Some researchers also extended the room temperature HE models (e.g. HEDE, HELP and HESIV) to account for the H-induced damage behavior at high temperatures [168,174], although no rigorous proof for the rationality of such extension has been established. Xiong et al. [179] have studied the effects of H on strain-induced vacancies at γ/γ' interfaces of a Ni-based superalloy using molecular dynamics (MD) method. They concluded that the H enhanced strain-induced vacancy formation is less prominent at higher temperatures for a constant pre-charged H concentration. This result provides an interesting example demonstrating the temperature-induced difference in H-defect interactions that must be considered when interpreting the HE behavior at elevated temperatures.

Hydrogen-induced damage at cryogenic temperatures

Due to its high specific energy content, liquid hydrogen (LH_2) has emerged as an alternative fuel for current aerospace application (e.g. launch vehicles) and future long-flight-duration aircraft. Reliable infrastructures like H tanks and the associated lines, tubes and other attachments are thus needed. Commonly used metallic materials for LH_2 storage include austenitic stainless steels and Al alloys [180]. These FCC materials do not suffer from ductile-to-brittle transitions at cryogenic temperatures even down to −253 °C (LH_2 temperature). Due to the almost immobile nature of H atoms at extremely low temperatures (e.g. −253 °C), damaging induced by H atoms seem not likely to occur at these temperature regimes. This is supported by Figs. 16(a) and (b) [181,182], which demonstrates the tensile and fatigue property of a AISI 304 L steel exposed to high-pressure H_2 gas or He gas at various temperatures. It is shown from these figures that the tensile and fatigue behavior of the tested steel is hardly affected by H at near LH_2 temperature. Similar results have also been reported from some other types of austenitic stainless steels, Al alloys, pure Ti and Ti alloys [181,183–185]. However, the HE behavior at the LH_2 temperature cannot be extended to all cryogenic temperature ranges. In fact, for common austenitic stainless steels (e.g. AISI 304 and 316), the HE effect becomes most severe at temperatures of around 50~150 °C below the room temperature (as shown in Fig. 14(a) and Fig. 16(c)). This is associated with the higher amount of deformation-induced martensite formation at cryogenic temperatures compared with that at the room temperature, due to the reduced austenite mechanical stability [186]. Compared with the austenite matrix, the transformed fresh martensite phase and the associated heterointerfaces are more easily attacked by H atoms that are still mobile at this temperature range [7,54].

For some materials like ferritic alloys that experience low-temperature induced embrittlement, the embrittling effects caused by cryogenic temperature and H can be superimposed. This is particularly true for the cases where stress-driven HEDE mechanism is dominant for H embrittlement. Fig. 17 provides two such examples, one from an austenite-ferrite two-phase lightweight steel [29] and the other from an austenitic high-Mn steel containing grain boundary κ-carbide [187]. In both steels, after H pre-charging and tensile testing, a clear brittle fracture behavior was observed, characterized by the ferrite cleavage cracking in the two-phase lightweight steel (Fig. 17(a)) and by the intergranular cracking in the austenitic high-Mn steel (Fig. 17(c)). Such cracking behavior was proposed to be due to the HEDE effect along ferrite {100} planes in the former steel and along the interface between grain-boundary κ-carbides and austenite matrix in the latter material. The damage features and the corresponding fractography in these H-charged and fractured specimens were very similar to those of the specimens loaded under liquid nitrogen temperature without the presence of H (Figs. 17(b) and (d)). Such similarity suggested that in these samples, the same damage behavior can be activated by both harsh environments, despite different underlying mechanisms. The reduced temperature increases the critical stress for dislocation gliding and H reduces the cohesive strength of crystal planes or interfaces [29,187]; cracking occurs when the former stress surpasses the latter. The superimposing effect of H environment and cryogenic temperature on materials' embrittlement is also demonstrated in the work of Fassina et al. [188], who have performed Charpy impact tests for a quenched and tempered ferritic F22 steel that was H pre-charged. Their results showed that a decreased temperature can induce ductile-to-brittle in this alloy and the presence of H increased the transition temperature ~30 °C (Fig. 18).

Summary and outlook

The presented review summarized and discussed the HE behavior and mechanisms in typical materials used in the field of H energy. It is generally shown that despite extensive research efforts (from both multiscale experiments and simulation work) devoted to this topic, detailed studies are generally lacking especially in non-ferrous materials and at non-ambient-temperatures. Even at room temperature where the influence of H on alloys' mechanical property is very well characterized, the underlying mechanisms are still subjected to strong debates. We

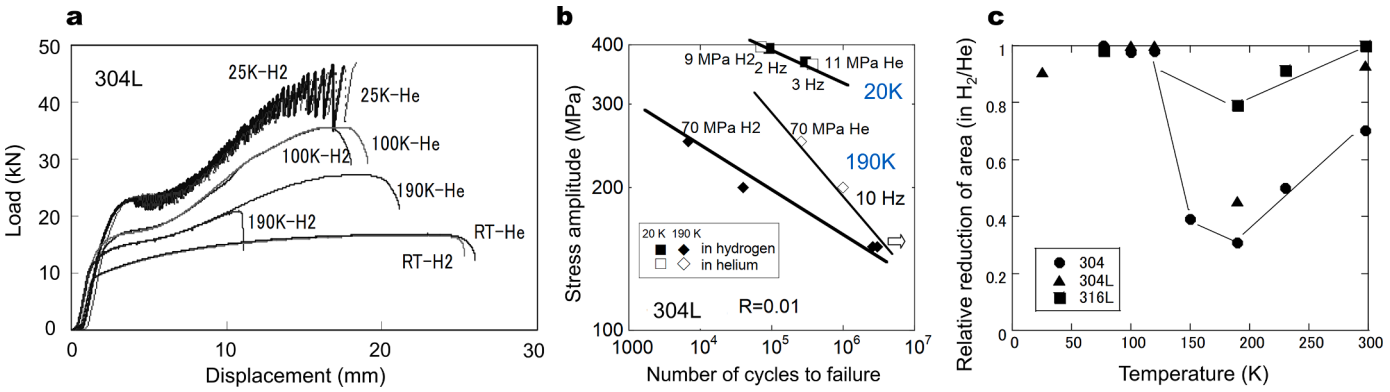

Fig. 16. (a) Tensile behavior of an AISI 304 L steel tested in 13 MPa H2 gas and 12 MPa He gas at different temperatures [181]; (b) Fatigue S-N curves of an AISI 304 L steel tested in high-pressure H2 or He gas at two different temperatures [182]; (c) Effect of testing temperature on the relative reduction of area (HE index) of AISI 304, 304 L, and 316 L in 13 MPa H2 gas and 12 MPa He gas [181].

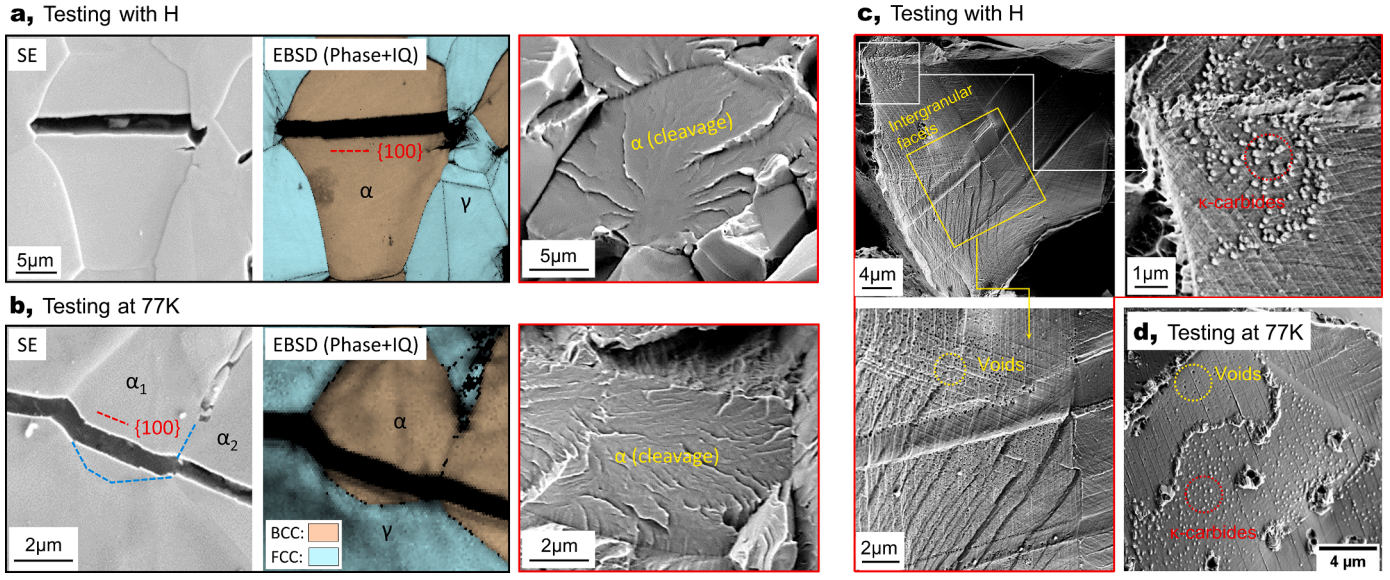

Fig. 17. Damage behavior and the corresponding fractography for a high-Mn high-Al two-phase lightweight steel (0.65C-19.7Mn-8.9Al, in wt.%) tested (a) with the presence of H and (b) under liquid nitrogen temperature without H [29]; Details on the intergranular facets of a fractured κ-carbide-containing high-Mn austenitic steel (1.3C-28.4Mn-8.3Al, in wt.%) subjected to (c) H pre-charging and tensile testing and (d) tensile testing at the liquid nitrogen without H charging [187].

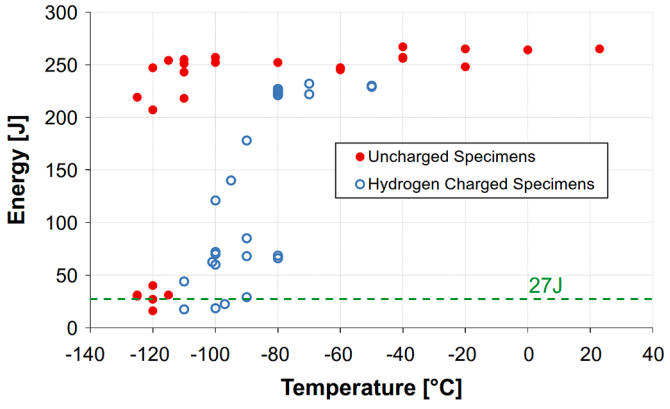

Fig. 18. The influence of testing temperature on Charpy impact energy of a quenched and tempered F22 steel with and without the presence of H [188].

believe the prevailing research challenges in comprehending HE include the following fours aspects: (a) the accurate characterization of H atoms (both trapped ones and diffusible ones), (b) the correct interpretation of the interplay between H and various lattice defects (vacancies, dislocations and interfaces) and its association with temperatures, (c) the identification and determination of the boundary conditions for the activation and prevalence of certain HE models and (d) the quantitative description between H-induced micro-damage and H-induced mechanical property degradation. The solution to these challenges is most likely the development of more advanced materials characterization techniques and modelling tools. Fortunately, HE can be mitigated without fully understanding the detailed mechanisms. To give an example, the migration of H atoms and their segregation to microstructural defects are believed to be the main reason for the occurrence of H-induced damage, regardless of the operating HE mechanisms (e.g. HELP or HEDE). As such, the introduction of second phase particles to trap H and thus to suppress its migration within the microstructure can be used as a method to enhance materials' HE resistance. This has indeed been proven to be effective in some cases. Therefore, great opportunities should be existed pertaining to the understanding of HE as well as the development of new strategies to overcome or mitigate this long-

standing issue, which can be simultaneously performed and advanced.

CRediT authorship contribution statement

Binhan Sun: Writing – review & editing, Writing – original draft, Investigation, Funding acquisition, Data curation, Conceptualization. **Huan Zhao:** Writing – original draft. **Xizhen Dong:** Writing – original draft. **Chaoyi Teng:** Writing – review & editing. **Aochen Zhang:** Writing – review & editing, Investigation. **Shuai Kong:** Writing – review & editing, Investigation. **Jingjing Zhou:** Writing – review & editing, Investigation. **Xian-Cheng Zhang:** Writing – review & editing, Supervision. **Shan-Tung Tu:** Writing – review & editing, Supervision, Project administration, Funding acquisition, Conceptualization.

Declaration of competing interest

The authors declare that they have no known competing financial interests or personal relationships that could have appeared to influence the work reported in this paper.

Data availability

Data will be made available on request.

Acknowledgement

This work was financially supported by the Science Center for Gas Turbine Project from China (Project No. P2022-C-III-002–001) and National Natural Science Foundation of China (No. 52275147), and carried out under the framework of “Integrated Research Platform for Greener Hydrogen Production and Utilization” sponsored by Ministry of Education.

References

[1] Rosen MA, Koohi-Fayegh S. The prospects for hydrogen as an energy carrier: an overview of hydrogen energy and hydrogen energy systems. Energy, Ecology and Environment 2016;1:10–29. https://doi.org/10.1007/s40974-016-0005-z.
[2] Bockris JOM. The hydrogen economy: Its history. Int J Hydrogen Energy 2013;38:2579–88. https://doi.org/10.1016/j.ijhydene.2012.12.026.
[3] S. Bouckaert, A.F. Pales. C. McGlade, et al. Net Zero by 2050: A Roadmap for the Global Energy Sector 2021.
[4] Sun B, Wang D, Lu X, et al. Current challenges and opportunities toward understanding hydrogen embrittlement mechanisms in advanced high-strength steels: a review. Acta Metallurgica Sinica (English Letters) 2021;34:741–54. https://doi.org/10.1007/s40195-021-01233-1.
[5] Nagao A, Smith CD, Dadfarnia M, et al. The role of hydrogen in hydrogen embrittlement fracture of lath martensitic steel. Acta Mater 2012;60:5182–9. https://doi.org/10.1016/j.actamat.2012.06.040.
[6] Neeraj T, Srinivasan R, Li J. Hydrogen embrittlement of ferritic steels: Observations on deformation microstructure, nanoscale dimples and failure by nanovoiding. Acta Mater 2012;60:5160–71. https://doi.org/10.1016/j.actamat.2012.06.014.
[7] Sun B, Krieger W, Rohwerder M, et al. Dependence of hydrogen embrittlement mechanisms on microstructure-driven hydrogen distribution in medium Mn steels. Acta Mater 2020;183:313–28. https://doi.org/10.1016/j.actamat.2019.11.029.
[8] Villalobos JC, Del-Pozo A, Vergara-Hernández HJ, et al. Hydrogen gaseous embrittlement effect over mechanical properties of an experimental X-120 microalloyed steel subjected to heat treatments and different cooling rates. Int J Hydrogen Energy 2022;47:30707–21. https://doi.org/10.1016/j.ijhydene.2022.07.042.
[9] Wang D, Hagen AB, Fathi P, et al. Investigation of hydrogen embrittlement behavior in X65 pipeline steel under different hydrogen charging conditions. Materials Science and Engineering: A 2022;860:144262. https://doi.org/10.1016/j.msea.2022.144262.
[10] Cheng H, Lu X, Zhou J, et al. The influence of L12 ordered precipitates on hydrogen embrittlement behavior in CoCrNi-based medium entropy alloys. Acta Mater 2023;260:119328. https://doi.org/10.1016/j.actamat.2023.119328.
[11] Lee JA. Hydrogen embrittlement. Hunstville, Alabama: NASA; April 2016.
[12] Rigas F, Amyotte P. Hydrogen safety. CRC Press; 2012.
[13] Johnson II WH. On some remarkable changes produced in iron and steel by the action of hydrogen and acids. Proc R Soc Lond 1875;23:168–79. https://doi.org/10.1098/rspl.1874.0024.
[14] San Marchi CW, Somerday BP. Technical reference for hydrogen compatibility of materials. Sandia National Laboratories (SNL), Albuquerque, NM, and Livermore, CA (United States) 2012.
[15] Zhao H, Chakraborty P, Ponge D, et al. Hydrogen trapping and embrittlement in high-strength Al alloys. Nature 2022;602:437–41. https://doi.org/10.1038/s41586-021-04343-z.
[16] Lee J. Hydrogen embrittlement of nickel, cobalt and iron-based superalloys. Gaseous hydrogen embrittlement of materials in energy. Technologies (Basel) 2012:624–67. https://doi.org/10.1533/9780857093899.3.624.
[17] Li X, Ma X, Zhang J, et al. Review of Hydrogen Embrittlement in Metals: Hydrogen Diffusion, Hydrogen Characterization, Hydrogen Embrittlement Mechanism and Prevention. Acta Metallurgica Sinica (English Letters) 2020;33:759–73. https://doi.org/10.1007/s40195-020-01039-7.
[18] Barrera O, Bombac D, Chen Y, et al. Understanding and mitigating hydrogen embrittlement of steels: a review of experimental, modelling and design progress from atomistic to continuum. J Mater Sci 2018;53:6251–90. https://doi.org/10.1007/s10853-017-1978-5.
[19] Dadfarnia M, Nagao A, Wang S, et al. Recent advances on hydrogen embrittlement of structural materials. Int J Fract 2015;196:223–43. https://doi.org/10.1007/s10704-015-0068-4.
[20] Bhadeshia HKDH. Prevention of hydrogen embrittlement in steels. ISIJ Int 2016;56:24–36. https://doi.org/10.2355/isijinternational.ISIJINT-2015-430.
[21] McMahon Jr C. Hydrogen-induced intergranular fracture of steels. Eng Fract Mech 2001;68:773–88. https://doi.org/10.1016/S0013-7944(00)00124-7.
[22] Martin ML, Dadfarnia M, Nagao A, et al. Enumeration of the hydrogen-enhanced localized plasticity mechanism for hydrogen embrittlement in structural materials. Acta Mater 2018.
[23] Nagumo M, Takai K. The predominant role of strain-induced vacancies in hydrogen embrittlement of steels: overview. Acta Mater 2019;165:722–33. https://doi.org/10.1016/j.actamat.2018.12.013.
[24] Lynch S. Hydrogen embrittlement (HE) phenomena and mechanisms, in Stress Corrosion Cracking. Elsevier 2011:90–130. https://doi.org/10.1533/9780857093769.1.90.
[25] Lynch S. Discussion of some recent literature on hydrogen-embrittlement mechanisms: addressing common misunderstandings. Corrosion Reviews 2019;37:377–95. https://doi.org/10.1515/corrrev-2019-0017.
[26] Sun B, Dong X, Wen J, et al. Microstructure design strategies to mitigate hydrogen embrittlement in metallic materials. Fatigue Fract Eng Mater Struct 2023;46:3060–76. https://doi.org/10.1111/ffe.14074.
[27] Oriani R. A mechanistic theory of hydrogen embrittlement of steels. Berichte der Bunsengesellschaft für physikalische Chemie 1972;76:848–57. https://doi.org/10.1002/bbpc.19720760864.
[28] Troiano AR. The role of hydrogen and other interstitials in the mechanical behavior of metals. Trans ASM 1960;52:54–80.
[29] Dong X, Wang D, Thoudden-Sukumar P, et al. Hydrogen-associated decohesion and localized plasticity in a high-Mn and high-Al two-phase lightweight steel. Acta Mater 2022:118296.
[30] Birnbaum HK, Sofronis P. Hydrogen-enhanced localized plasticity—A mechanism for hydrogen-related fracture. Materials Science and Engineering: A 1994;176:191–202. https://doi.org/10.1016/0921-5093(94)90975-X.
[31] Robertson I, Birnbaum H, Sofronis P. Hydrogen effects on plasticity. Dislocations in Solids 2009;15:249–93. https://doi.org/10.1016/S1572-4859(09)01504-6.
[32] Sofronis P, Birnbaum HK. Mechanics of the hydrogendashdislocationdashimpurity interactions—I. Increasing shear modulus. J Mech Phys Solids 1995;43:49–90. https://doi.org/10.1016/0022-5096(94)00056-B.
[33] Wang S, Hashimoto N, Ohnuki S. Hydrogen-induced change in core structures of {110}[111]edge and {110}[111]screw dislocations in iron. Sci Rep 2013;3:1–4. https://doi.org/10.1038/srep02760.
[34] Itakura M, Kaburaki H, Yamaguchi M, et al. The effect of hydrogen atoms on the screw dislocation mobility in bcc iron: a first-principles study. Acta Mater 2013;61:6857–67. https://doi.org/10.1016/j.actamat.2013.07.064.
[35] Nagumo M, Ohta K, Saitoh H. Deformation induced defects in iron revealed by thermal desorption spectroscopy of tritium. Scr Mater 1999;40. https://doi.org/10.1016/S1359-6462(98)00436-9.
[36] Nagumo M. Hydrogen related failure of steels–a new aspect. Materials Science and Technology 2004;20:940–50.
[37] Nagumo M, Nakamura M, Takai K. Hydrogen thermal desorption relevant to delayed-fracture susceptibility of high-strength steels. Metallurgical and Materials Transactions A 2001;32:339–47. https://doi.org/10.1007/s11661-001-0265-9.
[38] Djukic MB, Bakic GM, Zeravcic VS, et al. The synergistic action and interplay of hydrogen embrittlement mechanisms in steels and iron: Localized plasticity and decohesion. Eng Fract Mech 2019;216:106528. https://doi.org/10.1016/j.engfracmech.2019.106528.
[39] Novak P, Yuan R, Somerday B, et al. A statistical, physical-based, micro-mechanical model of hydrogen-induced intergranular fracture in steel. J Mech Phys Solids 2010;58:206–26. https://doi.org/10.1016/j.jmps.2009.10.005.
[40] Lynch S. Hydrogen embrittlement phenomena and mechanisms. Corrosion Reviews 2012;30:105–23. https://doi.org/10.1515/corrrev-2012-0502.
[41] Kirchheim R. Bulk diffusion-controlled thermal desorption spectroscopy with examples for hydrogen in iron. Metallurgical and Materials Transactions A 2016;47:672–96. https://doi.org/10.1007/s11661-015-3236-2.
[42] Ovejero-García J. Hydrogen microprint technique in the study of hydrogen in steels. J Mater Sci 1985;20:2623–9. https://doi.org/10.1007/BF00556094.

[43] Li K, Liu J, Grovenor CR, et al. NanoSIMS imaging and analysis in materials science. Annual Review of Analytical Chemistry 2020;13:273–92. https://doi.org/10.1146/annurev-anchem-092019-032524.

[44] Evers S, Senöz C, Rohwerder M. Hydrogen detection in metals: a review and introduction of a Kelvin probe approach. Sci Technol Adv Mater 2013. https://doi.org/10.1088/1468-6996/14/1/014201.

[45] Griesche A, Dabah E, Kannengießer T. Neutron imaging of hydrogen in iron and steel. Canadian Metallurgical Quarterly 2015;54:38–42. https://doi.org/10.1179/1879139514Y.0000000162.

[46] Breen AJ, Stephenson LT, Sun B, et al. Solute hydrogen and deuterium observed at the near atomic scale in high-strength steel. Acta Mater 2020;188:108–20. https://doi.org/10.1016/j.actamat.2020.02.004.

[47] Koyama M, Rohwerder M, Tasan CC, et al. Recent progress in microstructural hydrogen mapping in steels: quantification, kinetic analysis, and multi-scale characterisation. Materials Science and Technology 2017;33:1481–96. https://doi.org/10.1080/02670836.2017.1299276.

[48] Chen YS, Lu H, Liang J, et al. Observation of hydrogen trapping at dislocations, grain boundaries, and precipitates. Science (1979) 2020;367:171–5. https://doi.org/10.1126/science.aaz0122.

[49] Chang Y, Breen AJ, Tarzimoghadam Z, et al. Characterizing solute hydrogen and hydrides in pure and alloyed titanium at the atomic scale. Acta Mater 2018;150:273–80. https://doi.org/10.1016/j.actamat.2018.02.064.

[50] Yan F, Mouton I, Stephenson LT, et al. Atomic-scale investigation of hydrogen distribution in a TiMo alloy. Scr Mater 2019;162:321–5. https://doi.org/10.1016/j.scriptamat.2018.11.040.

[51] Hudson D, Cerezo A, Smith GD. Zirconium oxidation on the atomic scale. Ultramicroscopy 2009;109:667–71. https://doi.org/10.1016/j.ultramic.2008.10.020.

[52] Breen AJ, Mouton I, Lu W, et al. Atomic scale analysis of grain boundary deuteride growth front in Zircaloy-4. Scr Mater 2018;156:42–6. https://doi.org/10.1016/j.scriptamat.2018.06.044.

[53] Takahashi J, Kawakami K, Kobayashi Y, et al. The first direct observation of hydrogen trapping sites in TiC precipitation-hardening steel through atom probe tomography. Scr Mater 2010;63:261–4. https://doi.org/10.1016/j.scriptamat.2010.03.012.

[54] Sun B, Lu W, Gault B, et al. Chemical heterogeneity enhances hydrogen resistance in high-strength steels. Nat Mater 2021;20:1629–34. https://doi.org/10.1038/s41563-021-01050-y.

[55] Zhang B, Zhu Q, Xu C, et al. Atomic-scale insights on hydrogen trapping and exclusion at incoherent interfaces of nanoprecipitates in martensitic steels. Nat Commun 2022;13:1–11. https://doi.org/10.1038/s41467-022-31665-x.

[56] Senöz C, Evers S, Stratmann M, et al. Scanning Kelvin probe as a highly sensitive tool for detecting hydrogen permeation with high local resolution. Electrochem commun 2011;13:1542–5. https://doi.org/10.1016/j.elecom.2011.10.014.

[57] Robertson I. The effect of hydrogen on dislocation dynamics. Eng Fract Mech 1999;64:649–73. https://doi.org/10.1016/S0013-7944(99)00094-6.

[58] Tabata T, Birnbaum H. Direct observations of hydrogen enhanced crack propagation in iron. Scr Metall (United States) 1984;18. https://doi.org/10.1016/0036-9748(84)90513-1.

[59] Bond G, Robertson I, Birnbaum H. The influence of hydrogen on deformation and fracture processes in high-strength aluminum alloys. Acta Metallurgica 1987;35:2289–96. https://doi.org/10.1016/0001-6160(87)90076-9.

[60] Xie D, Li S, Li M, et al. Hydrogenated vacancies lock dislocations in aluminium. Nat Commun 2016;7:1–7. https://doi.org/10.1038/ncomms13341.

[61] Song J, Curtin W. Atomic mechanism and prediction of hydrogen embrittlement in iron. Nat Mater 2013;12:145–51. https://doi.org/10.1038/nmat3479.

[62] Song J, Curtin W. Mechanisms of hydrogen-enhanced localized plasticity: an atomistic study using α-Fe as a model system. Acta Mater 2014;68:61–9. https://doi.org/10.1016/j.actamat.2014.01.008.

[63] Tehranchi A, Curtin WA. The role of atomistic simulations in probing hydrogen effects on plasticity and embrittlement in metals. Eng Fract Mech 2019;216:106502. https://doi.org/10.1016/j.engfracmech.2019.106502.

[64] Shi H, Nandy S, Cheng H, et al. In-situ investigation of the interaction between hydrogen and stacking faults in a bulk austenitic steel. Acta Mater 2024;262:119441. https://doi.org/10.1016/j.actamat.2023.119441.

[65] Barnoush A, Vehoff H. Electrochemical nanoindentation: A new approach to probe hydrogen/deformation interaction. Scr Mater 2006;55:195–8. https://doi.org/10.1016/j.scriptamat.2006.03.041.

[66] Barnoush A, Vehoff H. Recent developments in the study of hydrogen embrittlement: Hydrogen effect on dislocation nucleation. Acta Mater 2010;58:5274–85. https://doi.org/10.1016/j.actamat.2010.05.057.

[67] Duarte MJ, Fang X, Rao J, et al. In situ nanoindentation during electrochemical hydrogen charging: a comparison between front-side and a novel back-side charging approach. J Mater Sci 2021;56:8732–44. https://doi.org/10.1007/s10853-020-05749-2.

[68] Wang D, Lu X, Deng Y, et al. Effect of hydrogen on nanomechanical properties in Fe-22Mn-0.6 C TWIP steel revealed by in-situ electrochemical nanoindentation. Acta Mater 2019;166:618–29. https://doi.org/10.1016/j.actamat.2018.12.055.

[69] Wang D, Lu X, Deng Y, et al. Effect of hydrogen-induced surface steps on the nanomechanical behavior of a CoCrFeMnNi high-entropy alloy revealed by in-situ electrochemical nanoindentation. Intermetallics (Barking) 2019;114:106605. https://doi.org/10.1016/j.intermet.2019.106605.

[70] Wang D, Lu X, Lin M, et al. Understanding the hydrogen effect on pop-in behavior of an equiatomic high-entropy alloy during in-situ nanoindentation. J Mater Sci Technol 2022;98:118–22. https://doi.org/10.1016/j.jmst.2021.04.060.

[71] Kirchheim R. Revisiting hydrogen embrittlement models and hydrogen-induced homogeneous nucleation of dislocations. Scr Mater 2010;62:67–70. https://doi.org/10.1016/j.scriptamat.2009.09.037.

[72] Kirchheim R. Reducing grain boundary, dislocation line and vacancy formation energies by solute segregation. I. Theoretical background. Acta Mater 2007;55:5129–38. https://doi.org/10.1016/j.actamat.2007.05.047.

[73] Kirchheim R. Reducing grain boundary, dislocation line and vacancy formation energies by solute segregation: II. Experimental evidence and consequences. Acta Mater 2007;55:5139–48. https://doi.org/10.1016/j.actamat.2007.05.033.

[74] Deng Y, Barnoush A. Hydrogen embrittlement revealed via novel in situ fracture experiments using notched micro-cantilever specimens. Acta Mater 2018;142:236–47. https://doi.org/10.1016/j.actamat.2017.09.057.

[75] Wan D, Deng Y, Meling JIH, et al. Hydrogen-enhanced fatigue crack growth in a single-edge notched tensile specimen under in-situ hydrogen charging inside an environmental scanning electron microscope. Acta Mater 2019;170:87–99. https://doi.org/10.1016/j.actamat.2019.03.032.

[76] Wang D, Hagen AB, Wan D, et al. Probing hydrogen effect on nanomechanical properties of X65 pipeline steel using in-situ electrochemical nanoindentation. Materials Science and Engineering: A 2021;824:141819. https://doi.org/10.1016/j.msea.2021.141819.

[77] Lawrence SK, Somerday BP, Ingraham MD, et al. Probing the effect of hydrogen on elastic properties and plastic deformation in nickel using nanoindentation and ultrasonic methods. JOM 2018;70:1068–73. https://doi.org/10.1007/s11837-018-2850-z.

[78] Huang L, Chen D, Xie D, et al. Quantitative tests revealing hydrogen-enhanced dislocation motion in α-iron. Nat Mater 2023:1–7. https://doi.org/10.1038/s41563-023-01537-w.

[79] Yin S, Cheng G, Chang TH, et al. Hydrogen embrittlement in metallic nanowires. Nat Commun 2019;10:1–9. https://doi.org/10.1038/s41467-019-10035-0.

[80] Abe JO, Popoola A, Ajenifuja E, et al. Hydrogen energy, economy and storage: review and recommendation. Int J Hydrogen Energy 2019;44:15072–86. https://doi.org/10.1016/j.ijhydene.2019.04.068.

[81] Michler T, Lindner M, Eberle U, et al. Assessing hydrogen embrittlement in automotive hydrogen tanks, in Gaseous hydrogen embrittlement of materials in energy technologies. Elsevier 2012:94–125. https://doi.org/10.1533/9780857093899.1.94.

[82] Yang C, Ogden J. Determining the lowest-cost hydrogen delivery mode. Int J Hydrogen Energy 2007;32:268–86. https://doi.org/10.1016/j.ijhydene.2006.05.009.

[83] Hawkins S, Joffe D. Technological characterisation of hydrogen storage and distribution technologies. Policy Studies Institute: London, UK 2006.

[84] Li H, Niu R, Li W, et al. Hydrogen in pipeline steels: Recent advances in characterization and embrittlement mitigation. J Nat Gas Sci Eng 2022:104709. https://doi.org/10.1016/j.jngse.2022.104709.

[85] Pacific Northwest National Laboratory. https://h2tools.org/hyarc/hydrogen-delivery.

[86] Rivard E, Trudeau M, Zaghib K. Hydrogen storage for mobility: a review. Materials 2019;12:1973. https://doi.org/10.3390/ma12121973.

[87] Barthélémy H. Hydrogen storage–Industrial prospectives. Int J Hydrogen Energy 2012;37:17364–72. https://doi.org/10.1016/j.ijhydene.2012.04.121.

[88] Wang Y, Hu S, Li Y, et al. Improved hydrogen embrittlement resistance after quenching–tempering treatment for a Cr-Mo-V high strength steel. Int J Hydrogen Energy 2019;44:29017–26. https://doi.org/10.1016/j.ijhydene.2019.09.142.

[89] Hosseini ZS, Dadfarnia M, Nibur KA, et al. Trapping against hydrogen embrittlement. In: Proceedings of the 2016 international hydrogen conference: materials performance in hydrogen environments. New York, NY: ASME Press; 2017. p. 71–80.

[90] Valentini R, Salina A. Influence of microstructure on hydrogen embrittlement behaviour of 2· 25Cr–1 Mo steel. Materials Science and Technology 1994;10:908–14. https://doi.org/10.1179/mst.1994.10.10.908.

[91] Martiniano GA, Leal JES, Rosa GS, et al. Effect of specific microstructures on hydrogen embrittlement susceptibility of a modified AISI 4130 steel. Int J Hydrogen Energy 2021;46:36539–56. https://doi.org/10.1016/j.ijhydene.2021.08.147.

[92] Michler T, Wackermann K, Schweizer F. Review and assessment of the effect of hydrogen gas pressure on the embrittlement of steels in gaseous hydrogen environment. Metals (Basel) 2021;11:637. https://doi.org/10.3390/met11040637.

[93] Connolly M, Martin M, Bradley P, et al. In situ high energy X-ray diffraction measurement of strain and dislocation density ahead of crack tips grown in hydrogen. Acta Mater 2019;180:272–86. https://doi.org/10.1016/j.actamat.2019.09.020.

[94] Shang J, Hua Z, Xing B, et al. Enhanced hydrogen embrittlement of steel by the premature hydrogen dissociation with the increasing inert gas pressure in hydrogen-containing mixtures. Acta Mater 2023:119279. https://doi.org/10.1016/j.actamat.2023.119279.

[95] Shang J, Chen W, Zheng J, et al. Enhanced hydrogen embrittlement of low-carbon steel to natural gas/hydrogen mixtures. Scr Mater 2020;189:67–71. https://doi.org/10.1016/j.scriptamat.2020.08.011.

[96] Zhou C, He Y, Jiang J, et al. Hydrogen uptake induced by CO_2 enhances hydrogen embrittlement of iron in hydrogen blended natural gas. Corros Sci 2022;207:110594. https://doi.org/10.1016/j.corsci.2022.110594.

[97] Komoda R, Yamada K, Kubota M, et al. The inhibitory effect of carbon monoxide contained in hydrogen gas environment on hydrogen-accelerated fatigue crack growth and its loading frequency dependency. Int J Hydrogen Energy 2019;44:29007–16. https://doi.org/10.1016/j.ijhydene.2019.09.146.

[98] Shibata A, Yonemura T, Momotani Y, et al. Effects of local stress, strain, and hydrogen content on hydrogen-related fracture behavior in low-carbon martensitic steel. Acta Mater 2021;210:116828. https://doi.org/10.1016/j.actamat.2021.116828.
[99] Momotani Y, Shibata A, Terada D, et al. Effect of strain rate on hydrogen embrittlement in low-carbon martensitic steel. Int J Hydrogen Energy 2017;42:3371–9. https://doi.org/10.1016/j.ijhydene.2016.09.188.
[100] Lynch S. A fractographic study of gaseous hydrogen embrittlement and liquid-metal embrittlement in a tempered-martensitic steel, in Perspectives in Hydrogen in Metals. Elsevier 1986:739–50. https://doi.org/10.1016/B978-0-08-034813-1.50103-0.
[101] Venezuela J, Liu Q, Zhang M, et al. A review of hydrogen embrittlement of martensitic advanced high-strength steels. Corrosion Reviews 2016;34:153–86. https://doi.org/10.1515/corrrev-2016-0006.
[102] Peral L, Zafra A, Belzunce J, et al. Effects of hydrogen on the fracture toughness of CrMo and CrMoV steels quenched and tempered at different temperatures. Int J Hydrogen Energy 2019;44:3953–65. https://doi.org/10.1016/j.ijhydene.2018.12.084.
[103] Loginow A, Phelps E. Steels for seamless hydrogen pressure vessels. Corrosion 1975;31:404–12. https://doi.org/10.5006/0010-9312-31.11.404.
[104] Liu Y, Wang M, Liu G. Effect of hydrogen on ductility of high strength 3Ni–Cr–Mo–V steels. Materials Science and Engineering: A 2014;594:40–7. https://doi.org/10.1016/j.msea.2013.11.058.
[105] Peral L, Zafra A, Fernández-Pariente I, et al. Effect of internal hydrogen on the tensile properties of different CrMo (V) steel grades: Influence of vanadium addition on hydrogen trapping and diffusion. Int J Hydrogen Energy 2020;45:22054–79. https://doi.org/10.1016/j.ijhydene.2020.05.228.
[106] Ohaeri E, Eduok U, Szpunar J. Hydrogen related degradation in pipeline steel: A review. Int J Hydrogen Energy 2018;43:14584–617. https://doi.org/10.1016/j.ijhydene.2018.06.064.
[107] Laureys A, Depraetere R, Cauwels M, et al. Use of existing steel pipeline infrastructure for gaseous hydrogen storage and transport: A review of factors affecting hydrogen induced degradation. J Nat Gas Sci Eng 2022;104534. https://doi.org/10.1016/j.jngse.2022.104534.
[108] Komoda R, Kubota M, Staykov A, et al. Inhibitory effect of oxygen on hydrogen-induced fracture of A333 pipe steel. Fatigue Fract Eng Mater Struct 2019;42:1387–401. https://doi.org/10.1111/ffe.12994.
[109] Martin M, Robertson I, Sofronis P. Interpreting hydrogen-induced fracture surfaces in terms of deformation processes: A new approach. Acta Mater 2011;59:3680–7. https://doi.org/10.1016/j.actamat.2011.03.002.
[110] Hattori M, Suzuki H, Seko Y, et al. The Role of Hydrogen-Enhanced Strain-Induced Lattice Defects on Hydrogen Embrittlement Susceptibility of X80 Pipeline Steel. JOM 2017;69:1375–80. https://doi.org/10.1007/s11837-017-2371-1.
[111] Mohtadi-Bonab MA, Szpunar JA, Basu R, et al. The mechanism of failure by hydrogen induced cracking in an acidic environment for API 5 L X70 pipeline steel. Int J Hydrogen Energy 2015;40:1096–107. https://doi.org/10.1016/j.ijhydene.2014.11.057.
[112] Martin ML, Fenske JA, Liu GS, et al. On the formation and nature of quasi-cleavage fracture surfaces in hydrogen embrittled steels. Acta Mater 2011;59:1601–6. https://doi.org/10.1016/j.actamat.2010.11.024.
[113] Nagumo M. Fundamentals of hydrogen embrittlement. Springer 2016:921.
[114] Martin M, Weber S, Theisen W, et al. Effect of alloying elements on hydrogen environment embrittlement of AISI type 304 austenitic stainless steel. Int J Hydrogen Energy 2011;36:15888–98. https://doi.org/10.1016/j.ijhydene.2011.09.013.
[115] Izawa C, Wagner S, Deutges M, et al. Relationship between hydrogen embrittlement and Md30 temperature: Prediction of low-nickel austenitic stainless steel's resistance. Int J Hydrogen Energy 2019;44:25064–75. https://doi.org/10.1016/j.ijhydene.2019.07.179.
[116] San Marchi C, Michler T, Nibur K, et al. On the physical differences between tensile testing of type 304 and 316 austenitic stainless steels with internal hydrogen and in external hydrogen. Int J Hydrogen Energy 2010;35:9736–45. https://doi.org/10.1016/j.ijhydene.2010.06.018.
[117] Sun B, Palanisamy D, Ponge D, et al. Revealing fracture mechanisms of medium manganese steels with and without delta-ferrite. Acta Mater 2019;164:683–96. https://doi.org/10.1016/j.actamat.2018.11.029.
[118] Sun B, Fazeli F, Scott C, et al. The influence of silicon additions on the deformation behavior of austenite-ferrite duplex medium manganese steels. Acta Mater 2018;148:249–62. https://doi.org/10.1016/j.actamat.2018.02.005.
[119] 清. 野原, 寛. 小野, and 延. 大橋. 準安定オーステナイトステンレス鋼における加工誘起マルテンサイト変態の組成および結晶粒度依存性. 鉄と鋼 1977;63:772–82. https://doi.org/10.2355/tetsutohagane1955.63.5_772.
[120] Ryu JH, Chun YS, Lee CS, et al. Effect of deformation on hydrogen trapping and effusion in TRIP-assisted steel. Acta Mater 2012;60:4085–92. https://doi.org/10.1016/j.actamat.2012.04.010.
[121] Perng T, Johnson M, Altstetter C. Influence of plastic deformation on hydrogen diffusion and permeation in stainless steels. Acta Metallurgica 1989;37:3393–7. https://doi.org/10.1016/0001-6160(89)90211-3.
[122] Koyama M, Abe Y, Saito K, et al. Martensitic transformation-induced hydrogen desorption characterized by utilizing cryogenic thermal desorption spectroscopy during cooling. Scr Mater 2016;122:50–3. https://doi.org/10.1016/j.scriptamat.2016.05.012.
[123] Hojo T, Koyama M, Terao N, et al. Transformation-assisted hydrogen desorption during deformation in steels: Examples of α′-and ε-Martensite. Int J Hydrogen Energy 2019;44:30472–7. https://doi.org/10.1016/j.ijhydene.2019.09.171.
[124] Pundt A, Kirchheim R. Hydrogen in metals: microstructural aspects. Annu Rev Mater Res 2006;36:555–608. https://doi.org/10.1146/annurev.matsci.36.090804.094451.
[125] Lee DH, Sun B, Lee S, et al. Comparative study of hydrogen embrittlement resistance between additively and conventionally manufactured 304 L austenitic stainless steels. Materials Science and Engineering: A 2021;803:140499. https://doi.org/10.1016/j.msea.2020.140499.
[126] Michler T, San Marchi C, Naumann J, et al. Hydrogen environment embrittlement of stable austenitic steels. Int J Hydrogen Energy 2012;37:16231–46. https://doi.org/10.1016/j.ijhydene.2012.08.071.
[127] Abraham DP, Altstetter CJ. Hydrogen-enhanced localization of plasticity in an austenitic stainless steel. Metallurgical and Materials Transactions A 1995;26:2859–71. https://doi.org/10.1007/BF02669644.
[128] Noh HS, Kang JH, Kim SJ. Effect of grain size on hydrogen embrittlement in stable austenitic high-Mn TWIP and high-N stainless steels. Int J Hydrogen Energy 2019;44:25076–90. https://doi.org/10.1016/j.ijhydene.2019.07.227.
[129] Noh HS, Kang JH, Kim KM, et al. The effect of carbon on hydrogen embrittlement in stable Cr-Ni-Mn-N austenitic stainless steels. Corros Sci 2017;124:63–70. https://doi.org/10.1016/j.corsci.2017.05.004.
[130] Nibur KA, Bahr DF, Somerday BP. Hydrogen effects on dislocation activity in austenitic stainless steel. Acta Mater 2006;54:2677–84. https://doi.org/10.1016/j.actamat.2006.02.007.
[131] Scully J, Young Jr G, Smith S. Hydrogen embrittlement of aluminum and aluminum-based alloys. Gaseous Hydrogen Embrittlement of Materials in Energy Technologies 2012:707–68. https://doi.org/10.1533/9780857093899.3.707.
[132] Wolverton C, Ozoliņš V, Asta M. Hydrogen in aluminum: First-principles calculations of structure and thermodynamics. Physical Review B 2004;69:144109. https://doi.org/10.1103/PhysRevB.69.144109.
[133] Larignon C, Alexis J, Andrieu E, et al. Investigation of Kelvin probe force microscopy efficiency for the detection of hydrogen ingress by cathodic charging in an aluminium alloy. Scr Mater 2013;68:479–82. https://doi.org/10.1016/j.scriptamat.2012.11.026.
[134] Charitidou E, Papapolymerou G, Haidemenopoulos G, et al. Characterization of trapped hydrogen in exfoliation corroded aluminium alloy 2024. Scr Mater 1999;41:1327–32. https://doi.org/10.1016/S1359-6462(99)00292-4.
[135] Anyalebechi PN. Hydrogen diffusion in Al-Li alloys. Metallurgical Transactions B 1990;21:649–55. https://doi.org/10.1007/BF02654243.
[136] Young GA, Scully JR. The diffusion and trapping of hydrogen in high purity aluminum. Acta Mater 1998;46:6337–49. https://doi.org/10.1016/S1359-6454(98)00333-4.
[137] Su H, Toda H, Shimizu K, et al. Assessment of hydrogen embrittlement via image-based techniques in Al–Zn–Mg–Cu aluminum alloys. Acta Mater 2019;176:96–108. https://doi.org/10.1016/j.actamat.2019.06.056.
[138] Su H, Toda H, Masunaga R, et al. Influence of hydrogen on strain localization and fracture behavior in Al Zn Mg Cu aluminum alloys. Acta Mater 2018;159:332–43. https://doi.org/10.1016/j.actamat.2018.08.024.
[139] Scamans GM, Holroyd NJH, Tuck CDS. The role of magnesium segregation in the intergranular stress corrosion cracking of aluminium alloys. Corros Sci 1987;27:329–47. https://doi.org/10.1016/0010-938X(87)90076-X.
[140] Song RG, Dietzel W, Zhang BJ, et al. Stress corrosion cracking and hydrogen embrittlement of an Al–Zn–Mg–Cu alloy. Acta Mater 2004;52:4727–43. https://doi.org/10.1016/j.actamat.2004.06.023.
[141] Wang Y, Sharma B, Xu Y, et al. Switching nanoprecipitates to resist hydrogen embrittlement in high-strength aluminum alloys. Nat Commun 2022;13:6860. https://doi.org/10.1038/s41467-022-34628-4.
[142] Albrecht J, Bernstein I, Thompson AW. Evidence for dislocation transport of hydrogen in aluminum. Metallurgical Transactions A 1982;13:811–20. https://doi.org/10.1007/BF02642394.
[143] Albrecht J, Thompson AW, Bernstein IM. The role of microstructure in hydrogen-assisted fracture of 7075 aluminum. Metallurgical Transactions A 1979;10:1759–66. https://doi.org/10.1007/BF02811712.
[144] Lu G, Kaxiras E. Hydrogen embrittlement of aluminum: the crucial role of vacancies. Phys Rev Lett 2005;94:155501. https://doi.org/10.1103/PhysRevLett.94.155501.
[145] Lu G, Kioussis N. Interaction of vacancies with a grain boundary in aluminum: A first-principles study. Physical Review B 2001;64:024101. https://doi.org/10.1103/PhysRevB.64.024101.
[146] Hara M, Domen K, Onishi T, et al. Formation and desorption of aluminum hydride from hydrogen adsorbed aluminum surfaces. Surf Sci 1991;242:459–63. https://doi.org/10.1016/0039-6028(91)90309-G.
[147] Winkler A, Resch C, Rendulic K. Aluminum hydride desorption from hydrogen covered aluminum single crystal surfaces. J Chem Phys 1991;95:7682–8. https://doi.org/10.1063/1.461342.
[148] Crane EL, Nuzzo RG. Collision-induced desorption and reaction on hydrogen-covered Al (111) single crystals: Hydrogen in aluminum? J Phys Chem B 2001;105:3052–61. https://doi.org/10.1021/jp003862v.
[149] Balasubramaniam R, Duquette D, Rajan K. On stress corrosion cracking in aluminum-lithium alloys. Acta Metallurgica et Materialia 1991;39:2597–605. https://doi.org/10.1016/0956-7151(91)90075-C.
[150] Balasooriya W, Clute C, Schrittesser B, et al. A Review on Applicability, Limitations, and Improvements of Polymeric Materials in High-Pressure Hydrogen Gas Atmospheres. Polymer Reviews 2022;62:175–209. https://doi.org/10.1080/15583724.2021.1897997.
[151] Alvine KJ, Kafentzis TA, Pitman SG, et al. An in situ tensile test apparatus for polymers in high pressure hydrogen. Review of Scientific Instruments 2014;85:8. https://doi.org/10.1063/1.4899315.

[152] Castagnet S, Grandidier JC, Comyn M, et al. Hydrogen influence on the tensile properties of mono and multi-layer polymers for gas distribution. Int J Hydrogen Energy 2010;35:7633–40. https://doi.org/10.1016/j.ijhydene.2010.04.155.
[153] Castagnet S, Grandidier JC, Comyn M, et al. Mechanical Testing of Polymers in Pressurized Hydrogen: Tension, Creep and Ductile Fracture. Exp Mech 2012;52:229–39. https://doi.org/10.1007/s11340-011-9484-1.
[154] Castagnet S, Grandidier JC, Comyn M, et al. Effect of long-term hydrogen exposure on the mechanical properties of polymers used for pipes and tested in pressurized hydrogen. Int J Press Vess Pip 2012;89:203–9. https://doi.org/10.1016/j.ijpvp.2011.11.008.
[155] Melnichuk M, Thiebaud F, Perreux D. Non-dimensional assessments to estimate decompression failure in polymers for hydrogen systems. Int J Hydrogen Energy 2020;45:6738–44. https://doi.org/10.1016/j.ijhydene.2019.12.107.
[156] Pepin J, Laine E, Grandidier JC, et al. Replication of liner collapse phenomenon observed in hyperbaric type IV hydrogen storage vessel by explosive decompression experiments. Int J Hydrogen Energy 2018;43:4671–80. https://doi.org/10.1016/j.ijhydene.2018.01.022.
[157] Pepin J, Laine E, Grandidier JC, et al. Determination of key parameters responsible for polymeric liner collapse in hyperbaric type IV hydrogen storage vessels. Int J Hydrogen Energy 2018;43:16386–99. https://doi.org/10.1016/j.ijhydene.2018.06.177.
[158] Zhang M, Lv H, Kang HR, et al. A literature review of failure prediction and analysis methods for composite high-pressure hydrogen storage tanks. Int J Hydrogen Energy 2019;44:25777–99. https://doi.org/10.1016/j.ijhydene.2019.08.001.
[159] Wang XL, Tian MM, Chen XD, et al. Advances on materials design and manufacture technology of plastic liner of type IV hydrogen storage vessel. Int J Hydrogen Energy 2022;47:8382–408. https://doi.org/10.1016/j.ijhydene.2021.12.198.
[160] Yamabe J, Nishimura S. Influence of fillers on hydrogen penetration properties and blister fracture of rubber composites for O-ring exposed to high-pressure hydrogen gas. Int J Hydrogen Energy 2009;34:1977–89. https://doi.org/10.1016/j.ijhydene.2008.11.105.
[161] Yamabe J, Nishimura S. EStimation of critical pressure of decompression failure of epdm composites for sealing under high-pressure hydrogen gas. 18th European Conference on Fracture: Fracture of Materials and Structures from Micro to Macro Scale ECF 2010;2010.
[162] Zheng YR, Tan Y, Zhou CL, et al. A review on effect of hydrogen on rubber seals used in the high-pressure hydrogen infrastructure. Int J Hydrogen Energy 2020;45:23721–38. https://doi.org/10.1016/j.ijhydene.2020.06.069.
[163] Yamabe J, Koga A, Nishimura S. Failure behavior of rubber O-ring under cyclic exposure to high-pressure hydrogen gas. Eng Fail Anal 2013;35:193–205. https://doi.org/10.1016/j.engfailanal.2013.01.034.
[164] Koga A, Uchida K, Yamabe J, et al. Evaluation on high-pressure hydrogen decompression failure of rubber O-ring using design of experiments. Int J Automot Eng 2011;2:123–9. https://doi.org/10.20485/jsaeijae.2.4_123.
[165] Poorhaydari K. A Comprehensive Examination of High-Temperature Hydrogen Attack—A Review of over a Century of Investigations. J Mater Eng Perform 2021;30:7875–908. https://doi.org/10.1007/s11665-021-06045-z.
[166] H. Malekmohammadi and M.H. Taghipour. A review on High Temperature Hydrogen Attack (HTHA) damage mechanisms, comparison and introduction of methods applicable for the detection of this phenomena. 2008.
[167] Fishgoit A, Kolachev B. Strength tests in hydrogen in the aerospace industry. Materials Science 1997;33:568–73. https://doi.org/10.1007/BF02537555.
[168] L Fritzemeier, W Chandler. Hydrogen embrittlement- Rocket engine applications. superalloys, supercomposites and superceramics(A 90-34151 14-26), 1989. San Diego, CA: Academic Press, Inc; 1989. p. 491–524.
[169] Michler T, Schweizer F, Wackermann K. Review on the influence of temperature upon hydrogen effects in structural alloys. Metals (Basel) 2021;11:423. https://doi.org/10.3390/met11030423.
[170] Boitsov I, Grishechkin S, Malkov I, et al. Physical and mechanical characteristics of EP741 and EP99 high-temperature nickel alloys in high-pressure hydrogen gas. Int J Hydrogen Energy 1999;24:919–26. https://doi.org/10.1016/S0360-3199(98)00168-2.
[171] J. Harris Jr and M. VanWanderham. Properties of materials in high pressure hydrogen at cryogenic, room, and elevated temperatures. 1973.
[172] Galliano F, Andrieu E, Blanc C, et al. Effect of trapping and temperature on the hydrogen embrittlement susceptibility of alloy 718. Materials Science and Engineering: A 2014;611:370–82. https://doi.org/10.1016/j.msea.2014.06.015.
[173] H.R. Gray. Hydrogen environment embrittlement. 1972.
[174] Huang S, Chen Z, Li Y, et al. Impact of hot bending on the high-temperature performance and hydrogen damage of 2.25 Cr-1Mo-0.25 V steel. J Mater Eng Perform 2019;28:567–77. https://doi.org/10.1007/s11665-018-3777-9.
[175] 誠. 福山, 東. 孫, 林. 張, et al. SUS316型ステンレス鋼の低温における水素環境脆化に及ぼす温度の影響. 日本金属学会誌 2003;67:456–9. https://doi.org/10.2320/jinstmet1952.67.9_45.
[176] He J, Han G, Fukuyama S, et al. Effect of hydrogen on dynamic precipitation of carbide in type 304 stainless steel during creep process. Acta Mater 1997;45:3377–88. https://doi.org/10.1016/S1359-6454(96)00400-4.
[177] Gahr S, Birnbaum HK. Hydrogen embrittlement of niobium—III. High temperature behavior. Acta Metallurgica 1978;26:1781–8. https://doi.org/10.1016/0001-6160(78)90089-5.
[178] Briant CL, Wang ZF, Chollocoop N. Hydrogen embrittlement of commercial purity titanium. Corros Sci 2002;44:1875–88. https://doi.org/10.1016/S0010-938X(01)00159-7.
[179] Xiong J, Zhu Y, Li Z, et al. Hydrogen-enhanced interfacial damage in Ni-based single crystal superalloy. Scr Mater 2018;143:30–4. https://doi.org/10.1016/j.scriptamat.2017.07.023.
[180] S.K. Mital, J.Z. Gyekenyesi, S.M. Arnold, et al. Review of current state of the art and key design issues with potential solutions for liquid hydrogen cryogenic storage tank structures for aircraft applications. 2006.
[181] Ogata T. Hydrogen embrittlement evaluation in tensile properties of stainless steels at cryogenic temperatures. AIP Conference Proceedings. American Institute of Physics 2008;986:124–31. https://doi.org/10.1063/1.2900335.
[182] Ogata T. Hydrogen environment embrittlement evaluation in fatigue properties of stainless steel SUS304L at cryogenic temperatures. AIP Conference Proceedings. American Institute of Physics 2010;1219:25–32. https://doi.org/10.1063/1.3402310.
[183] Markovich R, Schwartzberg F. Testing Techniques and Evaluation of Materials for Use at Liquid Hydrogen Temperature. Symposium on Evaluation of Metallic Materials in Design for Low-Temperature Service. ASTM International 1962.
[184] Yabumoto M, Yokogawa K, Ogata T, et al. Development of Cryogenic Materials for Liquid Hydrogen Transportation and Storage. J High Press Inst Jpn 2000;38:319–27. https://doi.org/10.11181/hpi1972.38.319.
[185] H. Fujii, J. Tanaka, S. Okaguchi, et al. Development of Cryogenic Materials Used for Liquid Hydrogen Transportation and Storage Vessels 2003. https://doi.org/10.2221/jcsj.38.212.
[186] Ogata T, Yuri T, Ono Y. Tensile Properties, Ferrite Contents, and Specimen Heating of Stainless Steels in Cryogenic Gas Tests. AIP Conference Proceedings. American Institute of Physics 2006. https://doi.org/10.1063/1.2192342.
[187] Elkot MN, Sun B, Zhou X, et al. Hydrogen-assisted decohesion associated with nanosized grain boundary κ-carbides in a high-Mn lightweight steel. Acta Mater 2022;241:118392. https://doi.org/10.1016/j.actamat.2022.118392.
[188] Fassina P, Bolzoni F, Fumagalli G, et al. Influence of hydrogen and low temperature on mechanical behaviour of two pipeline steels. Eng Fract Mech 2012;81:43–55. https://doi.org/10.1016/j.engfracmech.2011.09.016.